Journal of Nanobiotechnology

RESEARCH

Open Access

Polystyrene nanoplastics induce apoptosis, autophagy, and steroidogenesis disruption in granulosa cells to reduce oocyte quality and fertility by inhibiting the PI3K/AKT pathway in female mice

Yue Xue[1†], Xiu Cheng[1,3†], Zhang-Qiang Ma[1,3], Hou-Peng Wang[1,3], Chong Zhou[1], Jia Li[1], Da-Lei Zhang[1,3], Liao-Liao Hu[4], Yan-Fan Cui[2], Jian Huang[1], Tao Luo[2,3*] and Li-Ping Zheng[1,3*]

Abstract

Background Nanoplastics (NPs) are emerging pollutants that pose risks to living organisms. Recent findings have unveiled the reproductive harm caused by polystyrene nanoparticles (PS-NPs) in female animals, yet the intricate mechanism remains incompletely understood. Under this research, we investigated whether sustained exposure to PS-NPs at certain concentrations in vivo can enter oocytes through the zona pellucida or through other routes that affect female reproduction.

Results We show that PS-NPs disrupted ovarian functions and decreased oocyte quality, which may be a contributing factor to lower female fertility in mice. RNA sequencing of mouse ovaries illustrated that the PI3K-AKT signaling pathway emerged as the predominant environmental information processing pathway responding to PS-NPs. Western blotting results of ovaries in vivo and cells in vitro showed that PS-NPs deactivated PI3K-AKT signaling pathway by down-regulating the expression of PI3K and reducing AKT phosphorylation at the protein level, PI3K-AKT signaling pathway which was accompanied by the activation of autophagy and apoptosis and the disruption of steroidogenesis in granulosa cells. Since PS-NPs penetrate granulosa cells but not oocytes, we examined whether PS-NPs indirectly affect oocyte quality through granulosa cells using a granulosa cell–oocyte coculture system. Preincubation of granulosa cells with PS-NPs causes granulosa cell dysfunction, resulting in a decrease in the quality of the cocultured oocytes that can be reversed by the addition of 17β-estradiol.

[†]Yue Xue and Xiu Cheng contributed equally to this work.

*Correspondence:
Tao Luo
luotao@ncu.edu.cn
Li-Ping Zheng
Zhengliping@ncu.edu.cn

Full list of author information is available at the end of the article

Conclusions This study provides findings on how PS-NPs impact ovarian function and include transcriptome sequencing analysis of ovarian tissue. The study demonstrates that PS-NPs impair oocyte quality by altering the functioning of ovarian granulosa cells. Therefore, it is necessary to focus on the research on the effects of PS-NPs on female reproduction and the related methods that may mitigate their toxicity.

Highlights

- PS-NPs reduced oocyte quality and female fertility in mice.
- PS-NPs inhibited PI3K-AKT signaling pathway in mouse ovary and granulosa cells.
- PS-NPs decreased cell viability of granulosa cells by inducing apoptosis and autophagy.
- PS-NPs suppressed steroidogenesis of granulosa cells.
- PS-NPs reduced oocyte quality by causing granulosa cell dysfunction.

Keywords Apoptosis, Autophagy, Oocyte quality, PI3K/AKT signaling pathway, Polystyrene nanoplastics

Background

Currently, plastics permeate every facet of human existence, affording unparalleled convenience. However, given the challenges in their degradation and their widespread presence in the environment, plastic pollutants have become a significant environmental concern in modern times [1]. Following disposal into the environment, plastic waste undergoes degradation into smaller debris via an integration of chemical, physical, and biological mechanisms [2]. Thompson and colleagues were the first to introduce the term "microplastics (MPs) " to describe plastic debris measuring less than 5 mm [3]. Within the MPs realm, nanoplastics (NPs) are considered to be particles with a diameter smaller than 1 μm [4]. Micro/nanoparticles (MNPs) possess the capacity to disseminate extensively across diverse ecosystems [5]. Moreover, MNPs have the propensity to be readily assimilated and sequestered by living organisms, potentially perturbing the optimal operation of diverse tissues and organs as a result of their diminutive dimensions, resistance to degradation, and proclivity to amass hydrophobic organic contaminants [6]. Therefore, MNPs pollution is regarded as an emerging environmental issue.

Polystyrene (PS) is a prevalent plastic material globally, ranking among the top three polymers commonly detected in microplastic pollution in natural habitats [7, 8]. Its degradation is exceptionally challenging, leading to its prolonged persistence in the environment. Human exposure to PS-MNPs occurs routinely through ingestion, inhalation, and dermal contact on a daily basis due to their wide use in various aspects of human life [9, 10]. More importantly, PS-MNPs were observed in the circulatory system of humans and various organs, including the colon [11], lung [12, 13], placenta [14], and testis [15]. These results imply the potential hazard that PS-MNPs pose to human health. Given the intricate and vulnerable nature of the reproductive system to environmental pollutants, there has been a surge in research endeavors aimed at investigating the reproductive toxicity of PS-MNPs in both animal models [16, 17] and human cells [18]. Notably, PS-MNPs measuring less than 10 μm in diameter have demonstrated the ability to breach the blood-ovarian barrier and infiltrate the female reproductive system in mice [19–21]. These compounds cause programmed cell death and pyroptosis in ovarian granulosa cells, leading to fibrosis and injury in ovaries through the stimulation of inflammation and oxidative stress in both rats and mice [16, 19–26]. In addition, PS-NPs have been shown to diminish oocyte quality in mice [19], suggesting that PS-NPs may contribute to female infertility. Our recent study confirmed that PS-NPs reduce female fertility [21]. Nevertheless, the mechanisms through which PS-NPs diminish the quality of oocytes and female fertility are complicated and poorly understood. Our recent study revealed that PS-NPs mainly accumulate in granulosa cells in mouse ovaries [21]. Granulosa cells not only act as support cells for oocytes but also help oocytes grow and mature within follicles [27, 28]. Moreover, ovarian granulosa cells serve as specific cellular targets of PS-MNPs within the ovaries [16, 19–26]. Therefore, we hypothesize that PS-MNPs reduce oocyte quality and female fertility through adverse effects on granulosa cells.

In our research, female mice underwent in vivo exposure to diameter 25-nm PS-NPs, while ovarian granulosa cells were also treated with the 25-nm PS-NPs in vitro. Various parameters including female fertility, ovary index, estrous cycle, follicular development, oocyte quality, ovarian transcriptome, cell apoptosis and autophagy, molecular markers associated with apoptosis and autophagy, and PI3K-AKT signaling pathway were assessed. In addition, we evaluated whether PS-NPs affect oocyte quality through PS-NPs induced adverse effects on granulosa cells using a coculture system with mouse oocytes and PS-NPs treated granulosa cells in vitro. Our findings underscore the intricate interplay between granulosa cells and oocyte development, highlighting the critical importance of comprehending the influence of PS-NPs exposure on the reproductive health of female organisms.

Methods

Materials

PS-NPs (PS000025) and fluorescent PS-NPs (FPS-NPs, PSGF00020) were procured from Beijing Zhongkeleiming DaoJin Technology Co., Ltd. (Beijing, China). The subsequent reagents were acquired from Thermo Fisher Scientific Inc. (Wilmington, DE, USA): DMEM F/12 culture medium (C11330500BT), fetal bovine serum (FBS, 10270-106), 1% penicillin and streptomycin solution (15140148), TRlzol Reagent, and goat anti-rabbit secondary antibody conjugated with Alexa Fluor 594 (A-11012). Detailed information regarding the primary antibodies employed in our investigation is provided in Table S1. Tissue-Tek® Optimal Cutting Temperature (O.C.T.) compound (4583) was obtained from Sakura Finetek USA, Inc. (Torrance, CA, USA). Actin-Tracker Red-594 (C2205S) and 4',6-diamidino-2-phenylindole (DAPI) (C1005) were purchased from Beyotime Biotechnology (Shanghai, China). M2 culture medium (M7167), IBMX inhibitor (28822-58-4) and hyaluronidase (H4272) were sourced from Sigma−Aldrich (St. Louis, MO, USA). Bovine serum albumin (BSA, SW3015) and Wright Stain Solution (G1040) were obtained from Beijing Solarbio Science & Technology Co., Ltd. (Beijing, China), while Hematoxylin (AR1180-100) was procured from Boster Biological Technology Co., Ltd. (Wuhan, China).

Animals and ethics statement

Kun Ming (KM) mice were acquired from Royo Biotech Co., Ltd., located in Nanchang, China. These mice were housed in a specific pathogen-free facility, maintaining controlled conditions with temperatures maintained at approximately 22±2 ℃, relative humidity between 50 and 60%, and a consistent 12-hour light/dark cycle. They were provided ad libitum access to sterilized water and received a standard diet from Jiangsu Xietong Pharmaceutical Bioengineering Co., Ltd., based in Nanjing, China. The study adhered to ethical guidelines and obtained approval from the Institutional Animal Care and Use Committee of Royo Biotech Co., Ltd., under protocol number IACUC-RYE2021011301-1.

Study design

Recent studies [29, 30] estimate that an average person, weighing around 60 kg, consumes between 2.4 and 700 mg of plastic particles daily. To translate these human consumption rates to equivalent doses for mice, the dose-by-factor method, which accounts for differences in body surface area, was employed [31]. This method determined that the corresponding intake for a human would be in the range of 0.04 to 11.7 mg/kg, leading to a calculated mouse dose of about 0.5 to 144 mg/kg. Hence, for mice weighing 0.02 kg, the daily intake would be between 0.01 and 2.88 mg. In previous research by Zeng et al. [21], it was found that administration of 1 mg/day of PS-NPs led to a noteworthy decline in the reproductive capacities of female participants, aligning with concentrations found in environmental scenarios. Building upon this foundation, this current experiment divided thirty 4-week-old female KM mice into two distinct cohorts, each consisting of 15 individuals: one receiving daily oral gavage of sterile double distilled water (ddH_2O) as a control, and the other administered with 1 mg/day of PS-NPs. This regimen, delivering 0.1 ml of either substance for 42 consecutive days, was based on protocols established in earlier studies [21, 32]. The procedural methodology for this investigation is delineated in Fig. 1A.

After exposure for 28 days, vaginal smears of five mice from each group were examined every day for 2 weeks. A cotton swab or pipette was carefully inserted into the vaginal cavity of the mouse and softly twisted to gather cellular samples. The gathered cells were transferred onto a glass slide, allowed to dry in the air, fixed with methanol, stained with Wright Stain Solution, and imaged with an Olympus VYG-LED6FL microscope. The following criteria were employed to ascertain various phases of the estrous cycle. Proestrus is mainly composed of nucleated epithelial cells. The epidermis consists of many keratinized squamous epithelial cells that lack cell nuclei and have a flat and elongated shape. Metestrus contains a mixture of white blood cells, nucleated epithelial cells and some keratinized squamous epithelial cells. Diestrus is mainly composed of white blood cells.

After exposure for 42 days, a control female mouse and a PS-NPs exposed female mouse were mated with a fertile adult male mouse in a cage. In total, seven mating cages were used. The next day, evidence of successful mating was verified through the identification of vaginal plugs. The female mice that successfully copulated were kept for a duration of 21 days, and the size of their litters and number of implantation sites were examined. The implantation sites of 3 female mice from the control group or PS-NPs group were counted at 7.5 days after the occurrence of vaginal plugs. In addition, the litter magnitude of the neonatal mice was noted.

After 42 days of treatment, the female mice not in estrus period received an intraperitoneal injection of 10 international units (IU) of pregnant mare serum gonadotropin (PMSG) provided by Ningbo Sansheng Pharmaceutical Co., Ltd. This was followed 46–48 h later by another injection, this time of 10 IU of human chorionic gonadotropin (hCG), also sourced from Ningbo Sansheng Pharmaceutical Co., Ltd, with each injection volume being 100 μL per mouse. Subsequently, 13–14 h after the hCG injection, cumulus-oocytes complexs (COCs) were collected from the oviductal ampullae. Finally, 0.1% hyaluronidase is used to digest the granulosa cells on the COCs and release the oocytes. The collected oocytes

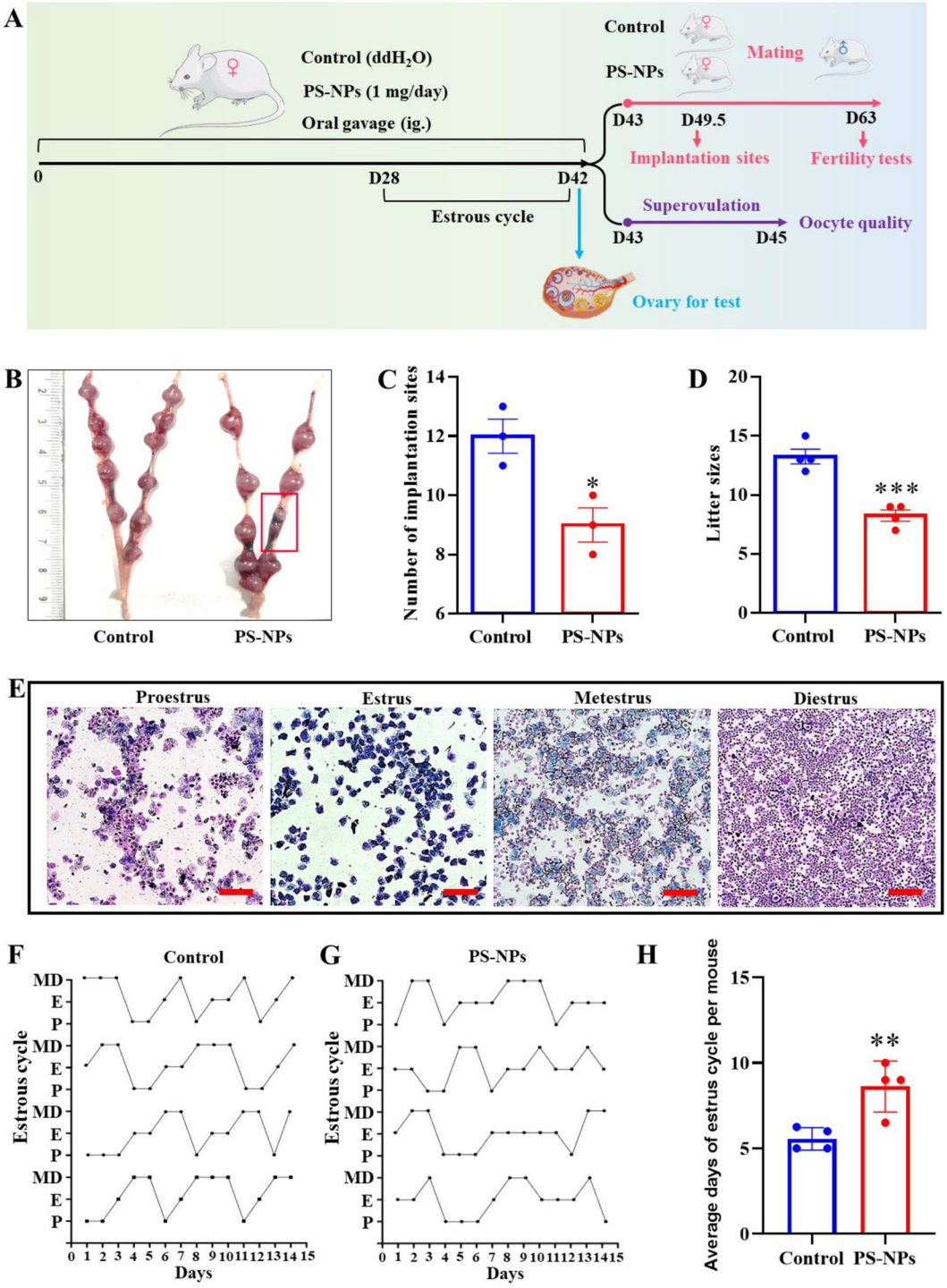

Fig. 1 Impact of PS-NPs on the reproductive health of female mice. (**A**) Schematic of the experimental procedure. (**B**) The typical morphology of the implantation site in mice subjected to PS-NPs exposure at 7.5 days of gestation. (**C**) Statistical analyses of the implantation sites in each group. The experiments were performed using three control and three PS-NPs exposed mice. (**D**) Statistical analyses of pups in each group. The experiments were performed using four control and four PS-NPs exposed mice. (**E**) The respective estrous cycles of mice in each group following exposure to PS-NPs. Bar: 50 μm. (**F**-**G**) Visual representation detailing the length of time associated with each phase of the estrous cycle. (**H**) Statistical evaluation of the average days of one estrous cycle in each mouse. The study involved four mice in the control group and four mice exposed to PS-NPs. The findings are expressed as mean ± SEM. Significance levels are indicated as $^{*}P < 0.05$, and $^{***}P < 0.001$, determined through the T-test

were then assessed for both the total ovulation number per mouse and the proportion that oocyte cytoplasmic fragmentation. Simultaneously, calculate the percentage of Metaphase II (MII) stage intact oocytes, which had released a polar body.

Analysis of PS-NPs properties

The morphology and configuration of the PS-NPs were scrutinized via a Hitachi H-600 transmission electron microscope situated in Tokyo, Japan. For the determination of the PS-NPs zeta potential and size distribution, a Zeta potential and particle size analyzer (ZetaPLUS) was utilized, with the analysis conducted in Brookhaven, New York City, NY, USA, under controlled conditions at 25 ℃.

Cell culture and treatments

For the acquisition of germ-vesicle (GV) stage oocytes, after euthanizing the female 8-week-old mice, the ovarium was removed and chopped under aseptic operation, and M2 culture medium containing 200 μM IBMX inhibitor was added to the culture dish, and GV stage oocytes were removed and cleaned with oral straws. GV stage oocytes were cultured in M2 medium with 100 μg/ml FPS-NPs for 12-h, with 10 GV stage oocytes per 20 μl M2 culture drop.

Granulosa cells were extracted from the ovaries of 5-week-old female KM mice using methods detailed in prior research [33]. In brief, KM mice injected intraperitoneally with 10 IU of PMSG were sacrificed, and the large follicles on the ovary were ruptured in M2 medium to release primary cumulus granulosa cells. The above tissue and cell suspension were collected and re-suspended by 40 μm cell filter (Biosharp, BS-40-CS), counted and cultured in 6-well plates (1×10^6 cells with 2mL medium) in DMEM F/12 supplemented with 10% FBS, 1% penicillin and streptomycin solution, 100 ng/mL testosterone, 0.05 IU/mL FSH, 0.05 IU/mL LH. These cells were then treated with PS-NPs in concentrations of 0, 50, 80, or 100 μg/mL with in above medium for a 24-hour period. Additionally, to assess the impact of PS-NP-triggered granulosa cell impairment on the quality of oocytes, granulosa cells underwent a 24-hour pretreatment with PS-NPs at a concentration of 80 μg/mL before being co-cultivated with oocytes. This was conducted within a granulosa cell-dependent system for oocyte maturation, a technique previously established and described [34, 35].

Ovarian index, histology, and follicular count

After exposure, the ovaries were collected and weighed in metestrus and diestrus (MD) period. The harvested ovaries underwent fixation in 4% paraformaldehyde before being embedded in paraffin, followed by the preparation of 5 μm thick sections. To process these ovarian sections, the paraffin was removed, and they were rehydrated using a sequence of xylene and ethanol washes, followed by staining with hematoxylin and eosin for visualization. Follicle counts were conducted to determine follicle density within the ovaries. This involved slicing six sections from each ovary at five different intervals and counting the total number of follicles across different developmental stages, encompassing primordial, primary, secondary, antral, atretic, and the cumulative follicle count.

Evaluation of oocyte oxidative stress and mitochondrial health

The presence of reactive oxygen species (ROS) within oocytes was identified using a ROS-sensitive fluorescein diacetate dye, employing an ROS detection kit (Catalogue S0033S, Beyotime Biotechnology, Shanghai, China), following the manufacturer's instructions. Similarly, the mitochondrial membrane potential (MMP) of the oocytes was assessed via a JC-1 assay kit (Catalogue C2006, Beyotime Biotechnology), following the manufacturer's recommended protocol.

RNA sequencing

RNA was isolated from the ovaries of three mice exposed to PS-NPs and three unexposed control mice using TRIzol reagent, following the manufacturer's instructions detailed in the product manual. For each sample, one microgram of RNA was prepared into sequencing libraries. These libraries underwent sequencing on an Illumina platform, generating paired-end sequences for subsequent analysis. The raw RNA sequencing (RNA-seq) data are accessible in the public domain via the National Center for Biotechnology Information under accession number PRJNA1060905. Initial data processing involved custom Perl scripts for cleaning the raw fastq files, which involved eliminating adapter sequences, poly-N sequences, and sequences of inferior quality to obtain pristine data. This process also involved calculating the Q30 (a quality score that denotes a 0.1% chance of an error and 99.9% confidence in the base call) and the GC content of the clean sequences. The analysis moved forward using only this high-quality, clean data. Alignment of the clean sequences to the mouse reference genome (Mus_musculus.GCF_000001635.27. genome.fa) was performed via HISAT2 software (version 2.0.4) [36, 37]. The alignment files were then processed to assemble the mapped reads using StringTie software [38].

Library quality control was examined by three quality examinations. First, fragment randomness and degradation of RNA samples were estimated by checking the distribution of mapped reads in the genome. Second, the length dispersion was examined by the length distribution of the inserts. The size of inserts was calculated as the distance between the start and end points on the reference genome in paired-end read mapping. Third,

the sufficiency of library volume (or mapped reads) was examined by generating a saturation curve between sampled mapped reads against genes identified within a certain range of expression accuracy.

Gene expression levels were quantified using the FPKM (Fragments Per Kilobase of transcript per Million mapped reads) approach, facilitated by StringTie using the max-flow algorithm [38]. To evaluate the consistency across biological replicates, Spearman's rank correlation coefficient and principal component analysis were applied. For identifying differentially expressed genes (DEGs), DESeq2 software (version 1.4.5) [39] was utilized, setting the criteria for significant differential expression at a fold change of 1.5 or more and a false discovery rate below 0.05. Annotation of these DEGs with Kyoto Encyclopedia of Genes and Genomes (KEGG) pathways was conducted through the KOBAS software [40], with the goal of categorizing the DEGs according to their associated biological pathways.

Quantitative real-time PCR

According to the manufacturer's instructions, total RNA was extracted from the ovaries of three mice subjected to PS-NPs treatment and three untreated control mice using TRIzol reagent. Subsequently, one microgram of this RNA was converted into cDNA through reverse transcription, and quantitative PCR (qPCR) analyses were carried out as outlined in previous descriptions. To quantify the expression levels of specific genes, the $2^{-\Delta\Delta Ct}$ approach was utilized, with gene expression normalized against the housekeeping gene *Gapdh*. Further information regarding the primer sequences utilized in this investigation is shown in Table S2.

Assessment of cell apoptosis and viability

Apoptosis in ovarian tissues was assessed utilizing the terminal deoxynucleotidyl transferase dUTP nick-end labeling (TUNEL) technique, as outlined in the accompanying instructions of the kit (Catalog #E-CK-A321, Elabscience Biotechnology, Inc., Wuhan, China). The apoptosis of granulosa cells was evaluated with an Annexin V/propidium iodide (PI) apoptosis detection kit (Catalog #E-CK-A211, Elabscience Biotechnology, Inc.), following the protocol provided by the manufacturer. Additionally, cell viability was assessed employing the Cell Counting Kit-8 (CCK-8) assay (Catalog #C6005M, US Everbright® Inc., Suzhou, China), strictly adhering to the manufacturer's guidelines.

Immunohistochemistry (IHC) and immunofluorescence (IF)

The localization and amount of ATG5 in the ovaries were examined via IHC [41]. Ovarian tissues from the control and PS-NPs treated groups were preserved in 4% paraformaldehyde for embedding in paraffin. These were then sectioned into 5 μm slices and placed on slides. Following this preparation, the sections underwent a series of treatments: they were first baked, then dewaxed and rehydrated. Antigen retrieval was carried out before the slides were blocked using a solution of phosphate-buffered saline (PBS) with 5% BSA added. They were then incubated with either an anti-ATG5 antibody or rabbit IgG (as a negative control), both diluted to 1:100 in a PBS solution containing 5% BSA, and kept at 4 °C throughout the night. To suppress endogenous peroxidase activity, the slides underwent treatment with 1% H_2O_2 at 37 ℃ for 10 min. After applying the secondary antibody, the peroxidase staining was developed using a DAB substrate kit (PV-6000D, ZSGBbio, Beijing, China). The slides were counterstained with hematoxylin, and differentiation was achieved with 0.1% hydrochloric acid. This was followed by a thorough rinse in tap water, a bluing process, dehydration through progressively concentrated ethanol solutions, clearing in xylene, and mounting with a neutral mountant. The slides were examined under an Olympus VYG-LED6FL microscope once dry.

The localization and amount of ATG5 in granulosa cells incubated with different concentrations of FPS-NPs were assessed using IF as described previously [41]. Mouse primary ovarian granulosa cells were exposed to concentrations of 0, 50, 80, or 100 μg/mL FPS-NPs for a duration of 24 h. Post-incubation, these cells were fixed using 4% paraformaldehyde for half an hour at a standard room temperature. Subsequent to fixation, a 0.2% Triton X-100 solution in PBS (PBST) was employed for cell permeabilization. The cells were then blocked using a 5% BSA solution in PBST before undergoing overnight incubation at 4℃ with either a rabbit IgG (used as a negative control at a dilution of 1:100) or an anti-ATG5 antibody (also at a dilution of 1:100). For the detection, cells were stained with an Alexa Fluor 594-conjugated goat anti-rabbit secondary antibody at a dilution of 1:600 for an hour and then with 1 μM DAPI for 30 min to highlight the nuclei. Fluorescence microscopy was performed to visualize the stained cells, using an Olympus VYG-LED6FL fluorescence microscope for the observation.

Accumulation of FPS-NPs in ovaries, granulosa cells, and oocytes

Female mice received oral administrations of 100 μl of a 10 mg/ml FPS-NPs solution and 100 μl of ddH_2O (serving as the negative control) daily. Three days following the last gavage, their ovaries were swiftly harvested and preserved by embedding in Tissue-Tek® O.C.T. compound, then instantly frozen using liquid nitrogen. Subsequently, these were sectioned into 5 μm slices with the aid of a CM1900 Leica thermostatic cryostat. The prepared ovarian slices were mounted on slides and treated with 1 μM DAPI for nuclear staining. Observations of these sections

were then conducted using a FV1000 Olympus laser scanning confocal microscope.

Ovarian granulosa cells, sourced primarily, were exposed to 100 μg/mL FPS-NPs or subjected to sterile ultrapure water (utilized as a negative control) over a 24-hour period. Following this incubation, they were stabilized using 4% paraformaldehyde for a duration of 20 min and then stained with Actin-Tracker Red-594 for 40 min at ambient temperature. Subsequent to rinsing, the cell nuclei underwent counterstaining with 1 μM DAPI. The resulting fluorescence distribution was then analyzed using an Olympus VYG-LED6FL fluorescence microscope.

Oocytes underwent a 24-hour incubation period with either 100 μg/mL FPS-NPs or sterile ultrapure water, serving as the negative control, and were subsequently examined under an Olympus VYG-LED6FL fluorescence microscope.

Western blotting

Protein extraction from both the ovaries of the PS-NPs and control groups, as well as from granulosa cells, was carried out. As outlined previously [21], western blotting was performed using 20 μg of protein from each sample. The primary antibodies and their respective dilution factors can be found in Table S1. The statistical evaluation of the target proteins was carried out by measuring the grayscale intensity of the bands recognized by specific antibodies. These measurements were then standardized against the bands detected by the anti-β-ACTIN antibody, which served as a reference for consistent loading. For this quantitative analysis, ImageJ software (version 1.44, developed by the National Institutes of Health) was utilized.

17β-estradiol (E2) detection

Following extraction of primary granulosa cells from mouse ovaries, these cells were seeded onto a 12-well plate at a density of 4×10^5 cells per well and cultured for 48 h in DMEM F/12 supplemented with 10% FBS, 1% penicillin and streptomycin solution, 100 ng/mL testosterone, 0.05 IU/ml FSH, 0.05 IU/ml LH to allow for cell adhesion. When assessing the effects of PS-NPs on E2 secretion by granulosa cells, 80 μg/mL PS-NPs were added to the cells in the medium described above for 24 h, followed by replacing the medium described above without FBS cultured for 24 h. The culture supernatant was collected to measure E2 levels. Serum E2 and granulosa cell-secreted E2 in the medium were detected by a QuicKey Pro Mouse E2 Kit (E-OSEL-M0008, Elabscience Biotechnology, Inc.) according to the user manual.

In vitro fertilization

Capacitated sperm were introduced to ovulated oocytes at a concentration of 4×10^5/ml in 100 μl of medium, followed by coincubation for 5 hours at 37 ℃ and 5% CO_2. Successful fertilization was confirmed by the presence of two pronuclei.

Statistical analyses

Data are expressed as the average value±the standard error of the mean (SEM). We employed the Shapiro-Wilk test to verify the normality of the data. The test results showed that the P value>0.05. To ascertain statistical significance, analysis was performed via either one-way ANOVA or the Student's t test (T-test). This data analysis utilized GraphPad Prism version 7.0 (GraphPad Software, based in San Diego, CA, USA). The P value<0.05 was deemed to reflect statistically significant differences.

Results

Exposure to PS-NPs decreases the reproductive capacity of female mice

Since our previous study revealed that PS-NPs induced ovarian dysfunction and reduced female fertility [21], we employed identical PS-NPs in this investigation to further elucidate the underlying mechanism involved. During this study, the size and zeta potential of the PS-NPs were meticulously measured, revealing that these NPs consistently maintained a spherical shape with an average diameter of about 25 nm and exhibited a zeta potential of -30 millivolts, as depicted in Fig. S1. Following PS-NPs exposure, the number of embryo implantation sites in the PS-NPs group exhibited lower than the control group 7.5 days after the occurrence of vaginal plugs, as shown in Fig. 1B and C. In addition, compared with control female mice, PS-NPs exposed female mice had a smaller litter size (Fig. 1D). Moreover, the findings from the vaginal cytology examination revealed that the control group demonstrated a consistent estrous cycle lasting between 5 and 6 days, whereas the PS-NPs group exhibited a prolonged estrous cycle (Fig. 1E-H).

Exposure to PS-NPs damages ovarian structure and function in female mice

The ovary ranks among the organs most susceptible to the effects of PS-MNPs. Previous studies, including one by Zeng et al. in 2023, highlighted the toxic impact of PS-NPs on mouse ovarian function. To further assess the ovarian toxicity attributed to PS-NPs, this research focused on evaluating the morphological and functional aspects of female mouse ovaries after PS-NPs exposure. These findings revealed that mice treated with PS-NPs had significantly smaller ovaries (Fig. 2A), lower ovarian weights (Fig. 2B), and decreased ovarian indices (Fig. 2C) in comparison to the control group in MD

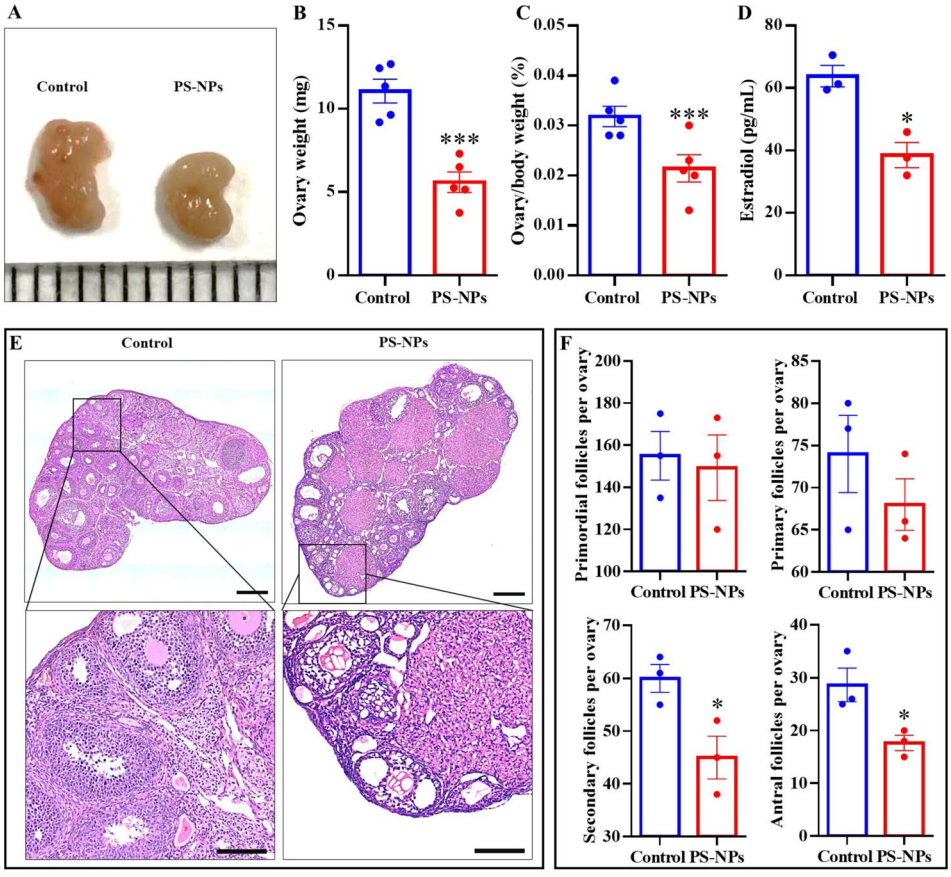

Fig. 2 Impact of PS-NPs on the ovarian structure of female mice. (**A**) Comparative ovarian morphology between control and PS-NPs-treated mice in MD period. Scale bar represents 1 mm. (**B**) Ovarian weight comparison between five control and five PS-NPs-treated mice. (**C**) Comparative analysis of ovarian indices in five control and five PS-NPs-exposed mice. (**D**) Comparison of serum E2 levels in three female mice exposed to PS-NPs and controls. (**E**) Histological comparison of ovarian structure in control and PS-NPs-exposed mice. Bar: 200 μm. (**F**) Analysis of follicle development stages in three mice from both groups.The evaluation metric is using the mean ± SEM. Significance levels indicated with $^{*}P < 0.05$ and $^{***}P < 0.001$, determined using T-test

period. Additionally, exposure to PS-NPs led to a drop in the serum E2 levels among the female mice (Fig. 2D). Histological examination showed that the mice were in the MD period, and the PS-NPs group had abnormal ovarian structure and reduced secondary and antral follicles compared to the control group (Fig. 2E and F). These observations suggest that PS-NPs have the potential to compromise ovarian integrity and function, hindering follicular development and hormonal synthesis, which may, in turn, impact female reproductive capacity negatively.

Impact of PS-NPs exposure on oocyte integrity in female mice

This section delves into the relationship between disrupted follicular development and its consequent effect on ovulation quality by analyzing the influence of PS-NPs on both the quantity and integrity of MII oocytes. Observations revealed a decrease in the ovulation number per mouse in the PS-NPs-treated group in contrast to the control group, but rate of MII oocytes not exhibit significant distinctions (Fig. 3A-B).Moreover, the PS-NPs exposed group showed more broken cytoplasmic oocytes than the control group (Fig. 3C). To assess the impact of PS-NPs on oocyte meiosis, GV-stage oocytes were cultured with PS-NPs at concentrations of 0, 50, 100, and 200 μg/mL. It was observed that the rates of GVBD and MII stage in the four groups of oocytes remained unaffected (Fig. S2). Furthermore, ovulation oocytes from the PS-NPs-treated group exhibited elevated levels of ROS and a decreased MMP in contrast to those from the control group (Fig. 3D-G). These findings suggest a deterioration in oocyte quality within the PS-NPs-exposed group. Consequently, it can be inferred that PS-NPs may trigger oxidative stress and impair mitochondrial functionality in oocytes, leading to a notable decline in their quality.

Identifying gene expression changes in mouse ovaries due to PS-NPs exposure

In an effort to further understand how PS-NPs influence female reproductive health, RNA-seq was conducted

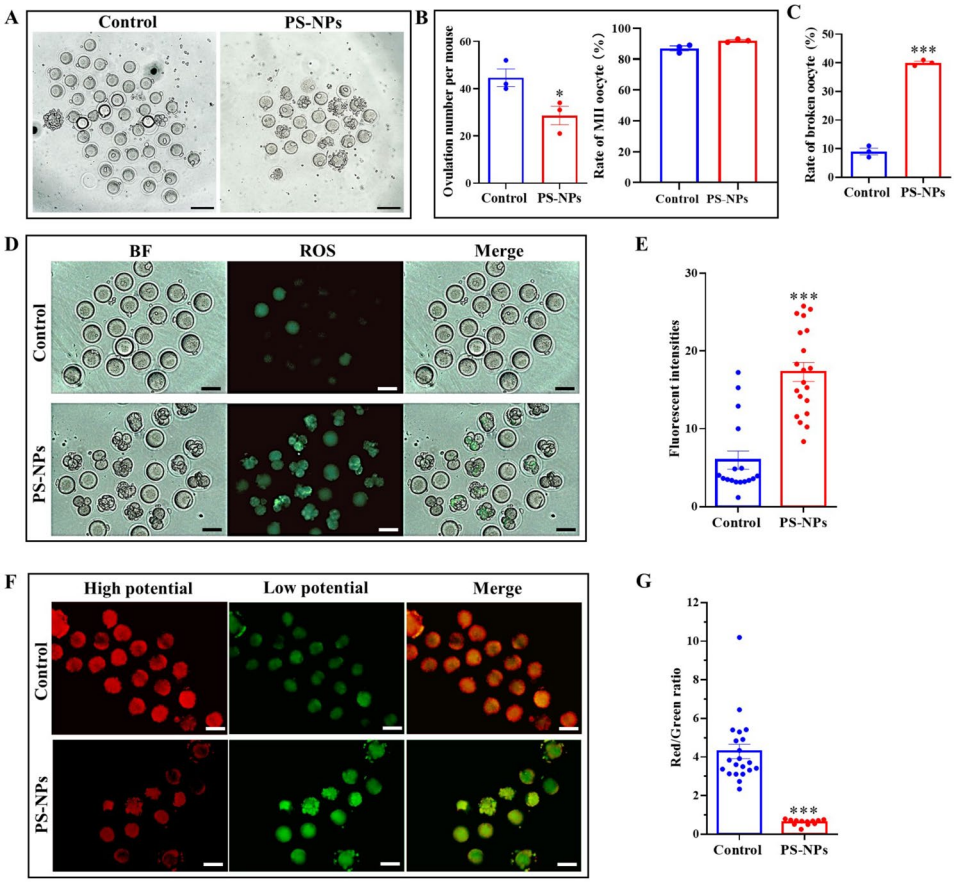

Fig. 3 Impact of PS-NPs exposure on mice oocyte quality. (**A**) Examination of oocyte morphology following superovulation in mice, comparing control groups with those exposed to PS-NPs. Bar: 100 μm. (**B** and **C**) Comparative statistics on the ovulation number per mouse, rate of MII oocytes and rate of broken oocyte. (**D**) Detection of ROS in MII oocytes from both three control and PS-NPs-treated mice, with green fluorescence indicating ROS presence. BF denotes bright field imaging. Bar: 100 μm. (**E**) Analysis of ROS levels in MII oocytes, measured comparatively. (**F**) Assessment of MMP in MII oocytes from the two groups. Bar: 100 μm. (**G**) Calculation of MMP via the ratio of red to green fluorescence intensity. Oocyte were collected from experiments on three mice per group (control and PS-NP-exposed). The evaluation metric is using the mean ± SEM, with significance indicated by $*P < 0.05$ and $***P < 0.001$, according to T-test

on ovarian tissue from both the control and PS-NPs-exposed groups. This analysis yielded 41.04 gigabases of high-quality data, with more than 93.07% of bases in each sample reaching a quality score of Q30 or higher (refer to Table S3). The alignment rate of each sample to the reference genome ranged from 93.77 to 94.88% (Table S3). In addition, the results of the mRNA fragmentation randomness check (Fig. S3), length distribution of inserts (Fig. S4), and saturation test (Fig. S5) showed that qualified libraries were constructed and used for RNA sequencing in this study. Spearman's correlation and principal component analysis showed good reproducibility of the biological replicates (Fig. S6). All these results indicate the good quality of the RNA-seq data.

In our investigation, 721 DEGs were discovered, comprising 353 genes that were upregulated and 368 that were downregulated, adhering to the defined criteria of exhibiting a fold change of at least 1.5 and a false discovery rate below 0.05 (see Fig. 4A and Table S4). The hierarchical clustering of these DEGs showcased the grouping of genes with similar expression patterns (refer to Fig. S7). Furthermore, the analysis leveraged KEGG to categorize the DEGs based on their associated pathways, aiming to identify the pathways that might contribute to the female reproductive toxicity induced by PS-NPs. The results showed that autophagy and apoptosis were two of the top 5 cellular processes associated with the upregulated genes (Fig. 4B and Table S4), suggesting that autophagy and apoptosis participate in PS-NPs induced ovarian dysfunction. In addition, among the downregulated genes, ovarian steroidogenesis was the second dominant pathway of organismal systems (Fig. 4C and Table S4), which may explain why PS-NPs impair hormone secretion from mouse ovaries (Fig. 2D). Additionally, within the realm of environmental information processing pathways, the PI3K-Akt signaling pathway was distinguished by having the highest count of downregulated genes (as shown in Fig. 4D and Table S4). Consequently,

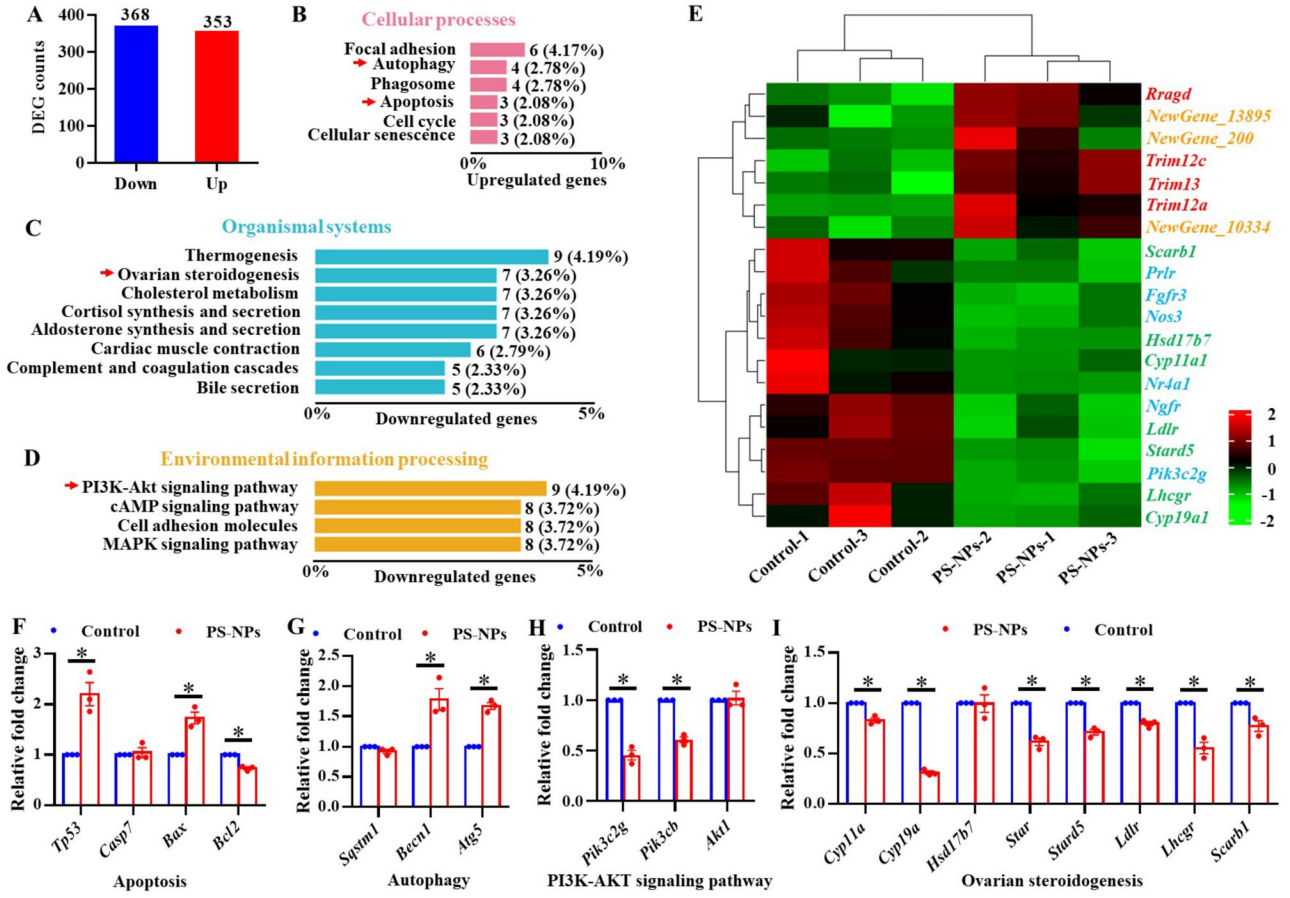

Fig. 4 Gene Expression Analysis via RNA-Seq to Explore the Ovarian Response to PS-NPs Exposure in Mice. (**A**) Overview of DEG statistics. The DEGs were annotated using the KEGG and categorized based on cellular processes (**B**), systems within organisms (**C**), and pathways for processing environmental information (**D**). (**E**) Hierarchical clustering showcases the expression patterns of DEGs involved in critical functions such as apoptosis, autophagy, PI3K-AKT signaling, and the regulation of ovarian steroidogenesis. (**F**-**I**) The expression levels of selected DEGs were validated through qPCR analysis. This step was conducted to corroborate the RNA-seq findings. The study included samples from three control and three PS-NPs-treated mice. Results are presented as mean ± SEM, with statistical significance denoted by $^{*}P < 0.05$, according to T-test

it is logical to proceed with a detailed investigation into the functional significance of these pathways in relation to the disrupted reproductive capabilities observed in female mice subjected to PS-NPs exposure.

A hierarchical clustering approach was utilized to analyze the DEGs associated with apoptosis, autophagy, the PI3K-AKT signaling pathway, and the regulation of ovarian steroidogenesis. This analysis identified genes with similar or related expression patterns and arranged them into clusters, highlighting a pattern of shared gene expression (see Fig. 4E). Additionally, qPCR was employed to confirm the expression levels of 18 critical genes within these pathways. The findings showed an upregulation in the expression of genes promoting apoptosis (such as *Tp53* and *Bax*) and autophagy (including *Becn1* and *Atg5*) in the ovarian tissue of mice exposed to PS-NPs in comparison to the control group (as depicted in Fig. 4F and G). Conversely, key genes integral to the PI3K-AKT signaling pathway (like *Pik3c2g* and *Pik3cb*) and those essential for ovarian steroidogenesis (such as *Cyp11a*, *Cyp19a*, *Star*, *Stard5*, *Ldlr*, *Lhcgr*, and *Scarb1*) exhibited significantly reduced expression in the PS-NPs-treated group's ovaries in comparison to the control group's (illustrated in Fig. 4H and I). These results confirmed the RNA-seq data and highlighted the transcriptional regulatory effect of these pathways on the molecular mechanisms underlying the female reproductive toxicity induced by PS-NPs.

Exposure to PS-NPs leads to the suppression of the PI3K-AKT signaling pathway and triggers apoptosis and autophagy in ovarian cells of female mice

Since the RNA-seq and qPCR results suggested the involvement of apoptosis and autophagy in PS-NPs-induced female reproductive toxicity, we investigated whether PS-NPs truly activate these cell death processes in ovaries. TUNEL assays highlighted increased apoptotic activity within the ovarian tissue of the PS-NPs-treated group, especially notable among the granulosa cells surrounding the follicles, in stark contrast to

the control group (see Fig. 5A). In parallel, there was a noticeable elevation in the levels of proapoptotic markers (P53, BAX, and cleaved Caspase-7) in the PS-NPs group compared to controls. Concurrently, the level of the antiapoptotic protein BCL2 and the BCL2/BAX ratio were found to be reduced in the ovaries from the PS-NPs cohort (illustrated in Fig. 5B-D). These results collectively suggest that PS-NPs promote apoptotic processes in the ovaries of mice.

Moreover, IHC targeting the autophagy marker ATG5 revealed significantly stronger staining in the ovarian tissues of the PS-NPs-treated mice, particularly within the granulosa cells, compared to the control group (Fig. 5E). This observation was substantiated by western blot analysis, which showed a rise in ATG5 protein levels in the PS-NPs group's ovaries (Fig. 5F and G). Additionally, a decrease in P62 levels, a lower LC3BI/LC3BII ratio, and an uptick in Beclin-1 expression were noted in the PS-NPs group, indicating enhanced autophagic activity in these ovaries (Fig. 5F-H). These discoveries align with the RNA-seq findings, underlining the induction of autophagy by PS-NPs in ovarian cells.

In parallel, the study investigated the expression levels of crucial components of the PI3K-AKT signaling pathway, including PI3K and AKT, through western blot analysis. This examination unveiled a decline in PI3K protein levels and a diminished ratio of phosphorylated AKT to total AKT (p-AKT/AKT) in the PS-NPs group compared to the control, consistent with the observed transcriptional downregulation of *Pi3k* and *Akt* (Figs. 4H and 5F and H). These results affirm the inhibition of the PI3K-AKT signaling pathway in the ovaries of mice exposed to PS-NPs, highlighting the pathway's involvement in mediating the effects of PS-NPs on promoting apoptosis and autophagy in ovarian tissue.

Predominant accumulation of PS-NPs in ovarian granulosa cells

Prior investigations have shown that PS-NPs are capable of accumulating within mouse ovarian tissue and

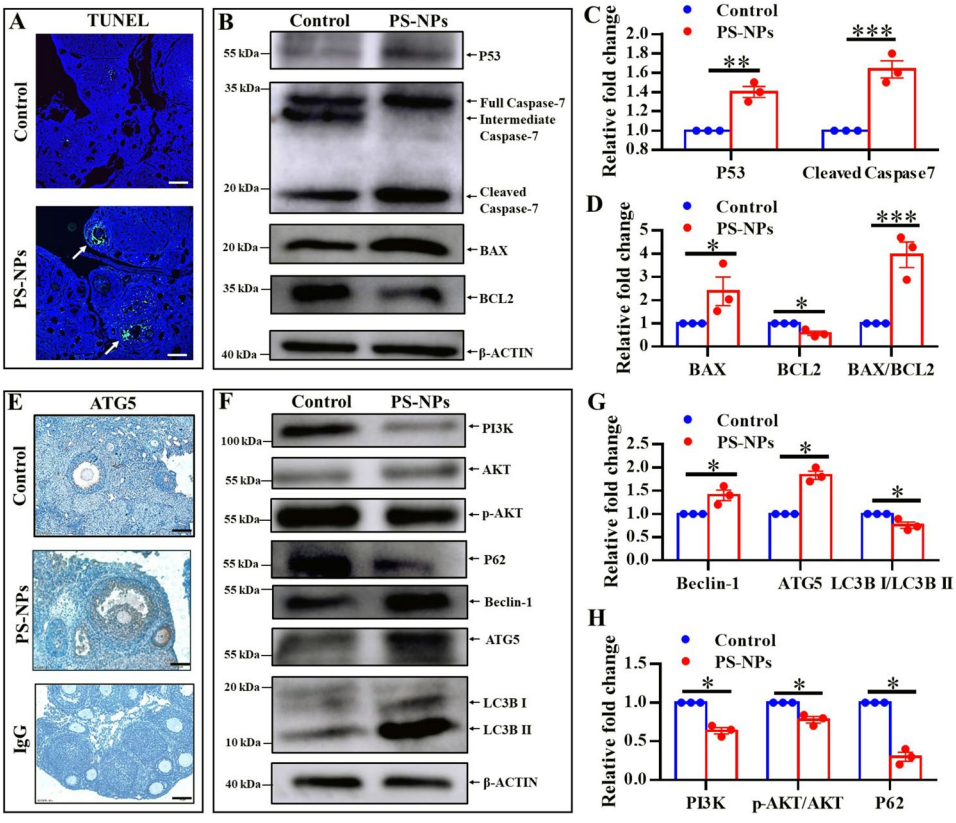

Fig. 5 Impact of PS-NPs exposure on apoptotic processes, autophagy activation, and PI3K-AKT pathway modulation in mouse ovarian tissue. (**A**) Detection of apoptotic cells in ovarian sections from both control and PS-NPs-treated mice, using TUNEL staining (apoptotic cells are marked with green fluorescence; apoptotic cells indicated with white arrows). Bar: 100 μm. (**B**) Apoptosis-inducing proteins in ovarian tissues from both groups were analyzed through western blotting. (**C** and **D**) Numerical analysis of proteins associated with apoptosis, as measured by western blotting. (**E**) Immunohistochemical staining for ATG5 in ovarian sections, comparing control and PS-NPs-treated mice. Bar: 100 μm. (**F**) Examination of autophagy-related and PI3K-AKT signaling proteins in ovarian tissues from both groups via western blotting. (**G** and **H**) Detailed quantification of autophagy and PI3K-AKT signaling proteins, as established through western blot analysis. This study included three mice in the control group and three exposed to PS-NPs. Results are presented as mean ± SEM, with significance levels of $^{*}P < 0.05$ and $^{***}P < 0.001$ determined using T-test

penetrating KGN cells [21], a human granulosa-like tumor cell line. The main goal of this research was to corroborate the presence of PS-NPs in mouse ovaries and evaluate their ability of PS-NPs to infiltrate primary granulosa cells and oocytes in mice. The findings revealed that PS-NPs primarily accumulated within the granulosa cells of mouse ovaries (Fig. 6A) and penetrated mouse primary granulosa cells cultured in vitro (Fig. 6B).

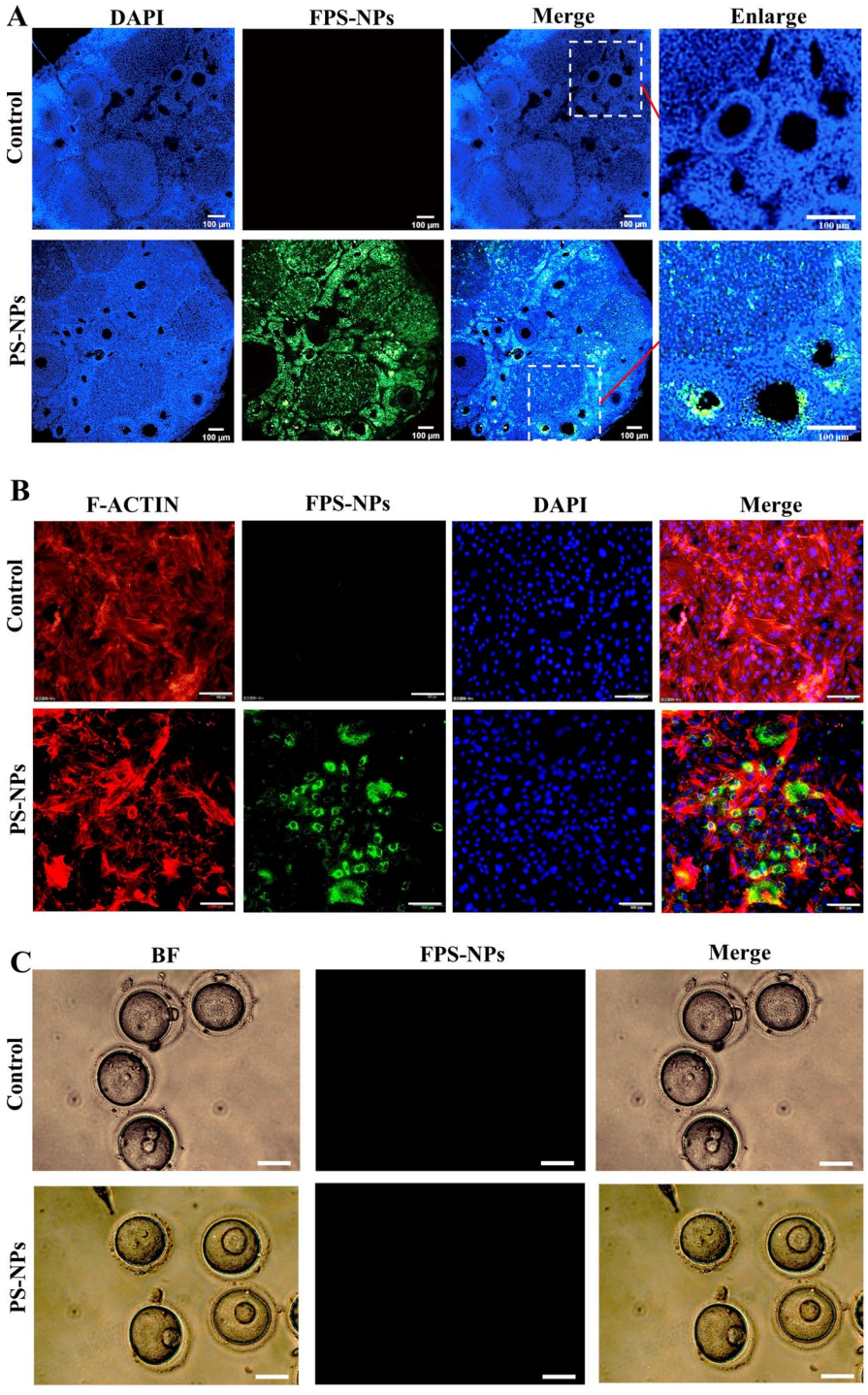

Fig. 6 Localization and Accumulation of PS-NPs in Mouse Ovarian Tissues, Granulosa Cells, and Oocytes. (**A**) Visualization of PS-NPs clusters within mouse ovarian tissue. Bar: 100 μm. (**B**) Detection of PS-NPs clusters in primary granulosa cells of mice. Bar: 100 μm. (**C**) GV stage oocytes were cultured with 0 and 100 μg/ml FPS-NPs in vitro for 12-hour and then the localization of MII stage oocytes FPS-NPs in oocytes was observed. Bar: 50 μm. These experiments were conducted in triplicate

However, PS-NPs could not penetrate the zone pellucida (ZP) into oocytes in either PS-NPs exposed mouse ovaries (Fig. 6A) or GV oocytes exposed to 100 μg /mL FPS-NPs in vitro 12-hour (Fig. 6C). These results indicate that ovarian granulosa cells are specific cellular targets of PS-NPs in ovaries.

PS-NPs exposure triggers apoptosis and autophagy while suppressing PI3K-AKT signaling in primary mouse granulosa cells

Due to the findings illustrated in Fig. 5, indicating a significant increase in apoptosis and autophagy within granulosa cells of PS-NPs exposed mice, and Fig. 6 revealing that PS-NPs fail to penetrate the ZP to reach oocytes but can infiltrate granulosa cells, these outcomes collectively suggest that granulosa cells may serve as pivotal targets for PS-NP-induced ovarian damage. To acquire a more comprehensive comprehension of the impacts of PS-NPs on granulosa cell function, this study utilized primary mouse granulosa cells. The results revealed a marked reduction in cell viability upon treatment with 80–100 μg/mL PS-NPs (Fig. S8A and B), whereas 50 μg/mL PS-NPs had negligible effects on cell apoptosis (Fig. S8A and B). Annexin-V/PI staining highlighted a notable increase in both early apoptotic cells (identified by Annexin-V positive, green fluorescence) and late apoptotic cells (PI positive, red fluorescence) upon treatment with 80 and 100 μg/mL PS-NPs (Fig. 7A-C).

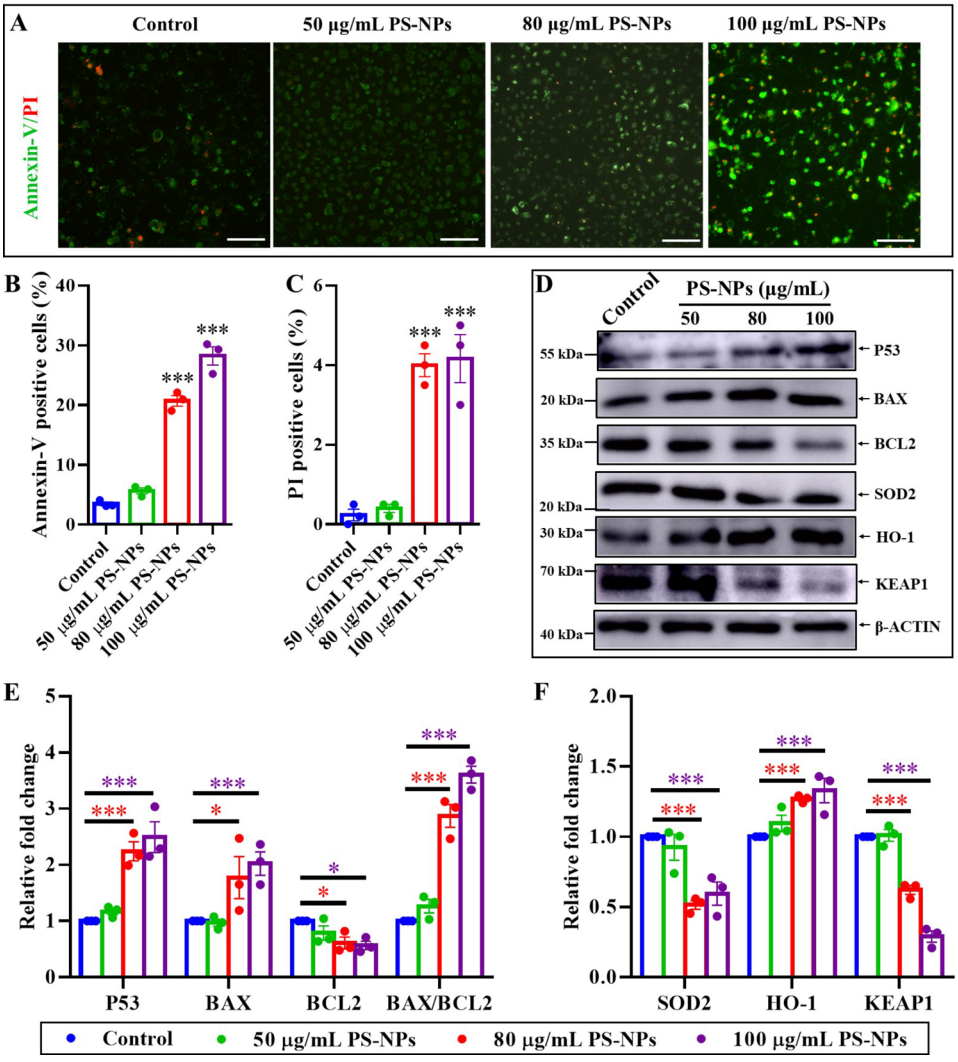

Fig. 7 Impact of PS-NPs Exposure on Apoptotic Processes in Primary Mouse Granulosa Cells. (**A**) Detection of apoptotic cells through Annexin-V/PI staining, where early and late stages of apoptosis are indicated by green and red fluorescence, respectively. Bar: 100 μm. (**B** and **C**) Quantitative analysis of cells positive for Annexin-V and PI staining. (**D**) Apoptosis-related protein levels were assessed in primary mouse granulosa cells exposed to PS-NPs compared to control cells, using western blot analysis. (**E** and **F**) Evaluation of PS-NPs effects on protein levels associated with apoptosis (**E**) and antioxidative responses (**F**). These analyses were performed in triplicate. Data are presented as mean ± SEM, with significance levels determined through one-way ANOVA and Dunnett's test, where $^{*}P < 0.05$ and $^{***}P < 0.001$

Furthermore, the exposure to these concentrations of PS-NPs led to elevated levels of apoptosis-inducing proteins P53 and BAX, and a reduction in BCL2, an anti-apoptotic protein, in primary mouse granulosa cells (Fig. 7D and E). The decreased BCL2/BAX ratio with 80 and 100 μg/mL PS-NPs treatment underscored an enhanced apoptotic response. Additionally, the levels of SOD2 and KEAP1 proteins were reduced, whereas HO-1 protein levels were increased in mouse primary granulosa cells exposed to 80 and 100 μg/mL PS-NPs (Fig. 7D and F), indicating that PS-NPs compromise redox stability and trigger oxidative stress within granulosa cells.

To evaluate the effect of PS-NPs on autophagy within mouse primary granulosa cells, ATG5 IF staining was conducted after incubating these cells with FPS-NPs. There was observed colocalization of ATG5 with PS-NPs within the cells, indicating an interaction (Fig. 8A). Furthermore, exposure to PS-NPs at concentrations of 80 and 100 μg/mL significantly intensified the IF signal of ATG5 (Fig. 8A and B), suggesting enhanced autophagy. This increase in autophagic activity was corroborated by western blot analysis, which showed a pronounced elevation in ATG5 protein levels in the primary granulosa cells from the mice (Fig. 8C and D). Furthermore, decreased P62, a reduced LC3BI/LC3BII ratio, and increased Beclin-1 were observed in mouse primary granulosa cells incubated with 80–100 μg/mL PS-NPs (Fig. 8C and D). These findings verified the capability of PS-NPs to activate autophagy in mouse primary granulosa cells, which was in line with the effect of PS-NPs on autophagy in mouse ovaries.

As a result of the suppression of the PI3K-AKT signaling pathway by PS-NPs in mouse ovaries, we validated whether PS-NPs suppressed this pathway in mouse primary granulosa cells. Consistent with the results in mouse ovaries, the levels of PI3K and p-AKT/AKT were markedly decreased in mouse primary granulosa cells incubated with 80–100 μg/mL PS-NPs (Fig. 8C and E). Moreover, it was observed that PS-NPs at concentrations of 80 and 100 μg/mL significantly reduced the protein levels of mTOR, an essential component of the PI3K-associated kinase family, highlighting a key interaction (Fig. 8C and E). This evidence strongly supports the conclusion that PS-NPs exposure in vitro adversely affects the PI3K-AKT signaling pathway in primary mouse granulosa cells.

PS-NPs reduce oocyte quality by causing granulosa cell dysfunction in a granulosa cell–oocyte coculture system

The research established an in vitro coculture framework incorporating both granulosa cells and oocytes, aiming to investigate the potential impact on oocyte quality resulting from dysfunction in granulosa cells induced by PS-NPs, as depicted in Fig. 9A. GV oocytes cocultured with normal primary granulosa cells underwent timely meiotic division, successfully extruding the first polar body (Fig. 9B and C). In contrast, coculture with granulosa cells preexposed to 80 μg/mL PS-NPs resulted in a significantly decreased rate of GVBD and MII oocyte (Fig. 9B and C). In addition, compared with those in oocytes cocultured with normal primary granulosa cells, ROS overaccumulated and the MMP decreased in oocytes cocultured with granulosa cells preexposed to 80 μg/mL PS-NPs (Fig. 9D-G). The in vitro fertilization rate was significantly lower when the oocytes were cocultured with granulosa cells preexposed to 80 μg/mL PS-NPs than when the oocytes were cocultured with normal primary granulosa cells (Fig. 9H and I). Such results indicate that PS-NPs caused granulosa cell dysfunction has a tangible impact on oocyte quality.

This research unveiled a decline in the expression levels of genes linked to estrogen production, like *Star*, *Cyp11a*, and *Cyp19a*, within the ovaries (as shown in Fig. 4), along with a lower serum E2 concentration in mice exposed to PS-NPs relative to those in the control group (as depicted in Fig. 2D). Given that the secretion of hormones is a crucial function of granulosa cells and theca cells in the ovary, especially that ovarian granulosa cells ultimately convert testosterone secreted by theca cells into E2. We examined whether PS-NPs affected the E2 secretion of mouse primary granulosa cells in the presence of testosterone. The exposure of mouse primary granulosa cells to PS-NPs at a concentration of 80 μg/mL led to a notable reduction in E2 levels within the culture supernatant, as highlighted in Fig. S8C. We also observed concurrent downregulation of *Cyp11a* and *Cyp19a* expression, yet an upregulation in *Hsd17b7* expression in Fig.S8D, suggesting a restriction in the conversion of testosterone to estrone. Furthermore, we added 70 pg/mL E2 to the culture supernatant of PS-NPs exposed granulosa cells to confirm whether the PS-NP-induced inhibition of E2 secretion was the cause of the low quality of the oocytes (Fig. 9A). This intervention resulted in a notable improvement in oocyte development with increased maturity (Fig. 9B and C). The compromised quality of oocytes caused by PS-NPs was also significantly improved, as shown by the reduced accumulation of ROS and increased MMP in the E2 intervention groups (Fig. 9D-G). Consequently, the in vitro fertilization rate was improved significantly by E2 treatment (Fig. 9H and I). These results emphasize the critical role granulosa cells play in maintaining oocyte integrity, proposing that the deterioration in oocyte quality and female fertility linked to PS-NPs is largely due to the compromised function of these cells.

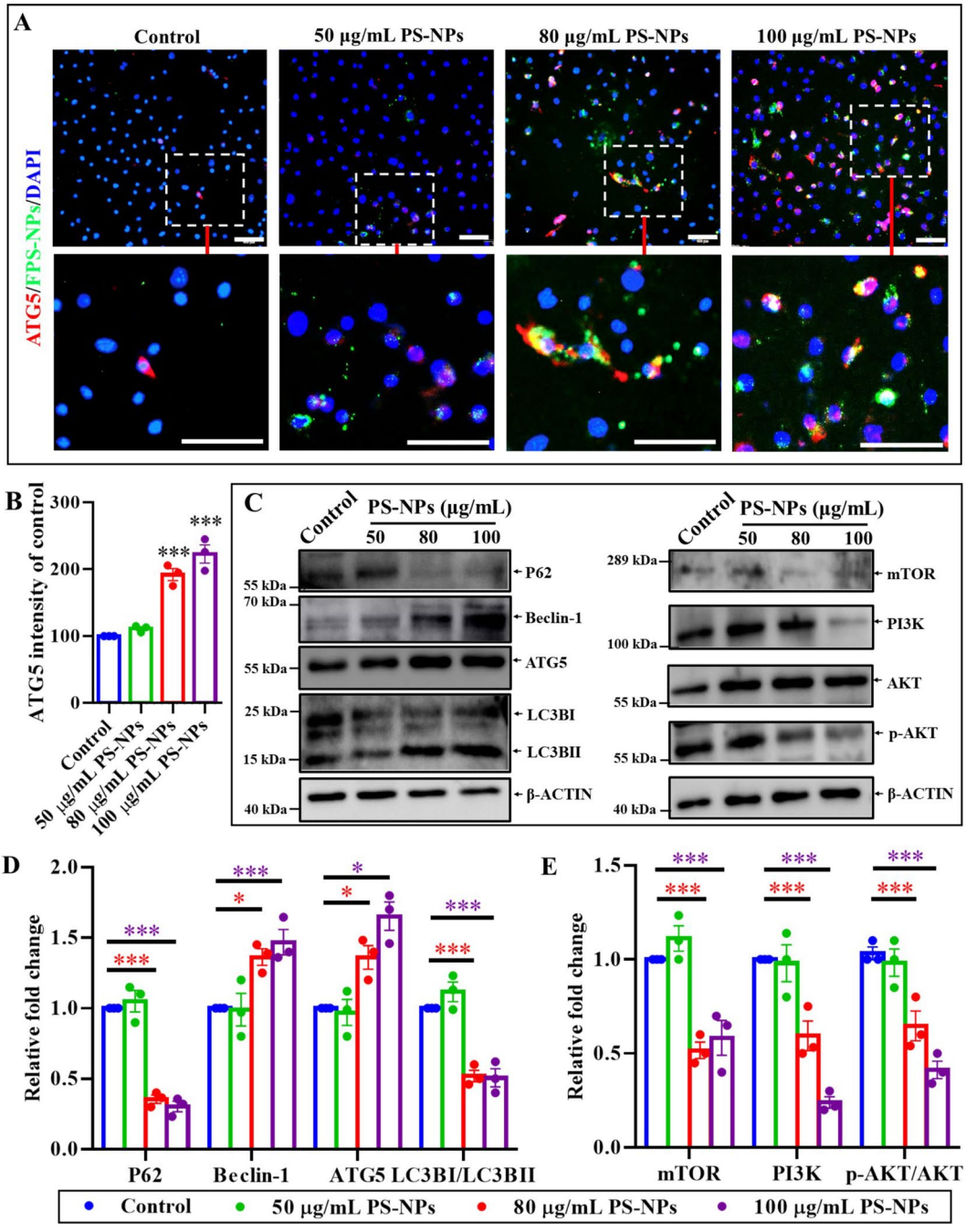

Fig. 8 Impact of PS-NPs on autophagy processes and PI3K-AKT pathway in mouse granulosa cells. (**A**) Visualization of ATG5 and PS-NPs colocalization through IF in primary mouse granulosa cells exposed to fluorescent PS-NPs. Bar: 100 μm. (**B**) Quantitative analysis of ATG5 fluorescence intensity. (**C**) Assessment of autophagy and PI3K-AKT signaling pathway protein levels via western blot in mouse granulosa cells after PS-NPs exposure compared to controls. (**D**) Evaluation of autophagy-related protein alterations due to PS-NP treatment. (**E**) Analysis of changes in PI3K-AKT SP proteins following PS-NP exposure, as depicted in Fig. 8C. These experiments were conducted in triplicate. Data are presented as mean ± SEM. Significant differences were identified using one-way ANOVA and Dunnett's test, with ***$P < 0.001$

Discussion

The reproductive system is among the most delicate and intricate systems in animals that respond to environmental pollutants. Recent investigations have uncovered the reproductive toxicity effects of PS-NPs on females, utilizing both rodent models and human cellular studies [16]. PS-NPs impair the structure and function of ovaries, cause dysfunction of ovarian granulosa cells, and compromise the quality of oocytes, consequently reducing female fertility [16]. However, the fundamental

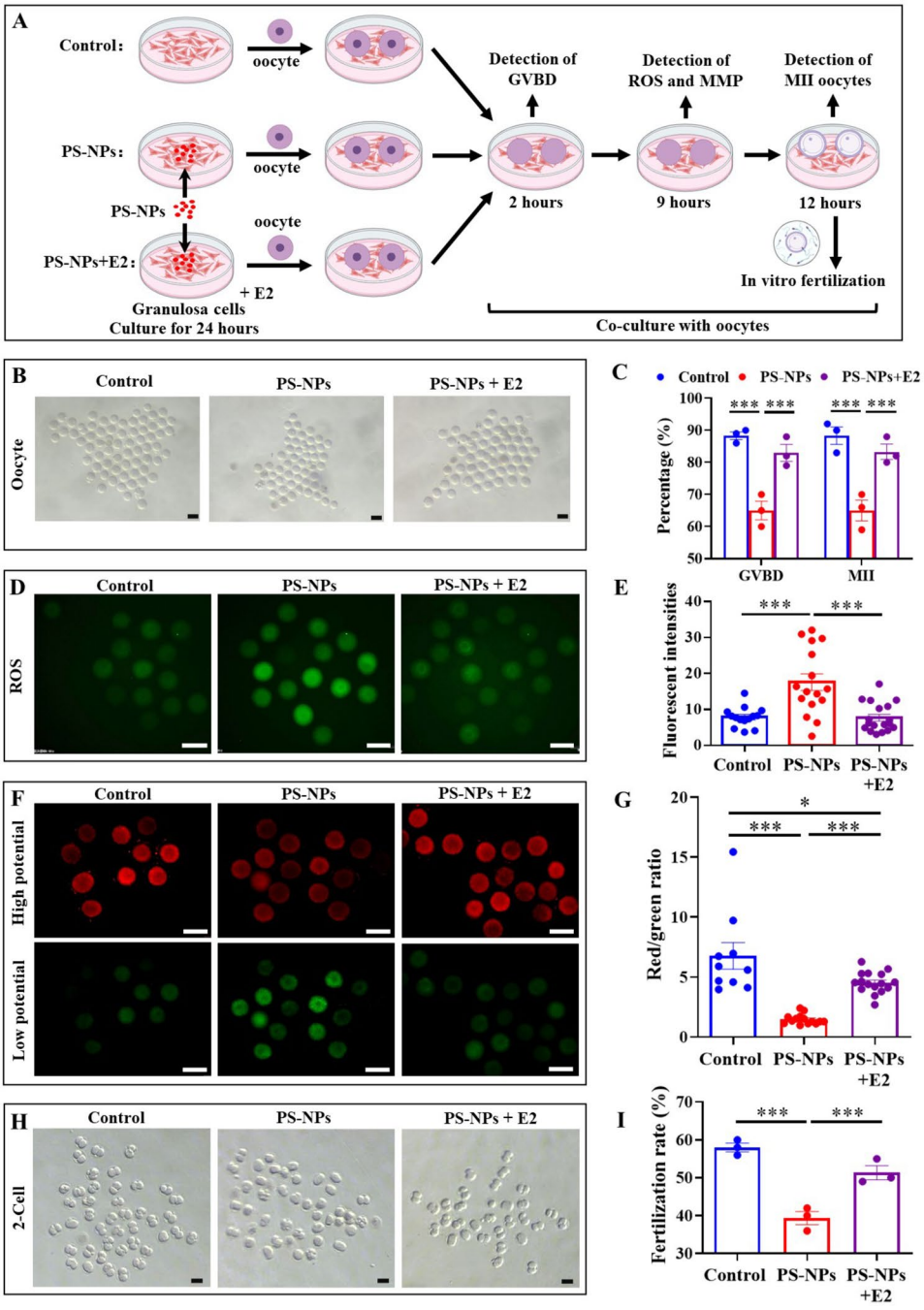

Fig. 9 PS-NPs indirectly affect oocyte quality through granulosa cells. (**A**) Mouse ovarian granulosa cells were preincubated with 80 μg/mL PS-NPs (PS-NPs) or ddH_2O (control) for 24 h. Then, the cell supernatant containing PS-NPs was discarded and added to the culture medium to co-culture the preprocessed granulosa cells with oocytes. For the 17β-Estradiol intervention (PS-NPs + E2), 70 pg/mL β-Estradiol was added to the co-culture system. The rate of GVBD and MII was recorded in control ($n = 66$), PS-NPs ($n = 52$), and PS-NPs + E2 ($n = 60$) groups after maturation for 2 -hours and 12-hours in vitro. (**B**) Oocyte morphology was assessed after coculture with preincubated granulosa cells. Bar: 100 μm. (**C**) GVBD and MII rates of oocytes in control, PS-NPs and PS-NPs + E2 groups. (**D**) ROS in MII oocytes cocultured with preincubated granulosa cells (green fluorescence represents ROS). Bar: 100 μm. (**E**) Quantification of the relative ROS levels in MII oocytes. (**F**) MMP of MII oocytes cocultured with preincubated granulosa cells. Bar: 100 μm. (**G**) Quantification of the MMP as the ratio of red to green fluorescence. (**H**) 2-cell-generated mouse embryos after in vitro fertilization using MII oocytes cocultured with preincubated granulosa cells. (**I**) Statistical analyses of 2-cell-generated mouse embryos after in vitro fertilization. Bar: 100 μm. These experiments were performed in three replicates. Results are presented as the mean ± SEM. Significance levels were determined using one-way ANOVA followed by Tukey's post-hoc test, with * indicating $p < 0.05$ and *** indicating $p < 0.001$. These experiments were conducted in triplicate. The data are expressed as mean ± SEM. Statistical significance was assessed via one-way ANOVA followed by Tukey's post-hoc test, with *$P < 0.05$ and *** $P < 0.001$

process has not been completely clarified. Our experimental findings revealed that exposure to PS-NPs compromised the viability and functionality of granulosa cells by triggering both apoptosis and autophagy processes. The dysfunction of granulosa cells, induced by PS-NPs, led to a deterioration in oocyte quality and a reduction in female fertility. Additionally, we identified the PI3K-AKT signaling pathway as a crucial mediator in the reproductive toxicity induced by PS-NPs in females. Our results provide a deeper insight into the negative effects of PS-NPs on female reproductive health.

Recent studies have identified several pathways through which PS-NPs impact the reproductive health of females. For instance, PS-NPs have been found to initiate cell death processes like pyroptosis and apoptosis in ovarian granulosa cells using the NLRP3/Caspase-1 pathway in female rats [24]. Furthermore, PS-NPs exposure has been linked to the activation of the Wnt/β-catenin signaling pathway, which has been correlated with ovarian fibrosis and the apoptosis of granulosa cells [22]. In our own previous research, we noted that PS-NPs led to oxidative stress and activated the Hippo signaling pathway in granulosa cells [21]. However, these investigations have not fully unraveled the complex underlying mechanisms through which PS-NPs exert their reproductive toxicity in females. Given the intricacy of the toxicity mechanism associated with PS-NPs, many additional pathways may be involved. This research utilized RNA seq to demonstrate that PS-NPs predominantly impact the PI3K-AKT signaling pathway, a critical route for processing environmental cues. The functionality of this signaling network is essential for the regulation of ovarian physiology, and disturbances within this complex system may contribute to reproductive [42–44] and early embryo development issues in females [45–48]. There have been reports indicating that ovarian autophagy is induced by suppression of the PI3K-AKT signaling cascade in rodent models [49], while the accrual of ROS and apoptosis in granulosa cells are inhibited by activation of this pathway in patients with PCOS [50]. Moreover, the inhibition of the PI3K-AKT signaling pathway was shown to disrupt steroid production in rat granulosa cells by diminishing the levels of *Star*, *P450scc*, and *3β-HSD* [51], whereas its activation enhanced E2 production by boosting the expression of genes implicated within E2 synthesis, such as *Star*, *Cyp11a1*, and *Cyp19a1*, in pig granulosa cells [52]. Such observations highlight the essential role of the PI3K-AKT signaling pathway in managing autophagy, maintaining ROS balance, triggering apoptosis, and regulating steroid synthesis within the ovary. A recent investigation by Zhang et al. [2]. revealed that the PI3K-AKT signaling pathway is instrumental in the DNA damage observed in sperm from male mice exposed to PS-NPs, emphasizing the pathway's contribution to the reproductive harms of PS-NPs. This research offers the first piece of evidence that PS-NPs deactivate the PI3K-AKT signaling pathway in both the ovaries and granulosa cells of mice, highlighting its significant role in the detrimental impacts on female reproductive health caused by PS-NPs.

We hypothesized that granulosa cells are the main cellular targets within the ovaries for PS-NPs, a notion corroborated by findings from earlier studies [16]. Given the essential functions of granulosa cells in hormone production, oocyte development, and the ovulation process [27, 28, 53], the detrimental impacts of PS-NPs on female fertility can be attributed to the disruption of granulosa cell function by PS-NPs. The PI3K-AKT signaling pathway is proposed to mediate the granulosa cell damage caused by PS-NPs through four distinct mechanisms, as detailed in Fig. 10. First, the deactivation of the PI3K-AKT signaling pathway by PS-NPs led to a decrease in mTOR activity, potentially reducing mTOR's suppression of autophagy and thereby triggering its activation. Of course, the levels of autophagy within granulosa cells profoundly impact their functionality. Suppression of autophagy can diminish the expression of genes associated with granulosa cell functions such as CYP19A1/aromatase and FSHR, consequently resulting in reduced E2 synthesis [54]. Induction of autophagy in granulosa cells by Bisphenol A can induce cellular dysfunction [55]. It is crucial to uphold an optimal equilibrium of autophagy within granulosa cells to ensure their proper functioning. Second, the exposure to PS-NPs led to enhanced levels of P53 following the pathway's inactivation. It's documented that P53 is pivotal in controlling oxidative stress and promoting cell death [56]. The stimulation of P53 is capable of initiating cell death processes in granulosa cells that have encountered PS-NPs. Given P53's role in suppressing the expression of SOD2, a key enzyme in defending against oxidative damage [57], the increase in P53 levels due to PS-NPs exposure could lead to decreased SOD2 protein levels, potentially disrupting the balance of ROS. Third, decreased AKT attenuated the inhibitory effects of BAX and Caspase 7 and the activation of BCL2, which upregulated BAX and Caspase 7 but downregulated BCL2, leading to apoptosis. Fourth, prior research has shown that blocking the PI3K-AKT signaling pathway diminishes steroid hormone production in rat granulosa cells [51]. In our current work, we have verified that PS-NPs decrease E2 levels by suppressing genes crucial for E2 production. It is worth noting that the synergistic action of the theca cells and granulosa cells plays a major role in E2 synthesis. Additionally, during follicular development, the theca cell, the granulosa cell layer and the ZP act as a protective barrier, preventing exogenous substances from entering the oocyte. Therefore, the theca cells and the granulosa cell layer are damaged before the oocyte. Previously reports that NPs mainly accumulate in the cytoplasm

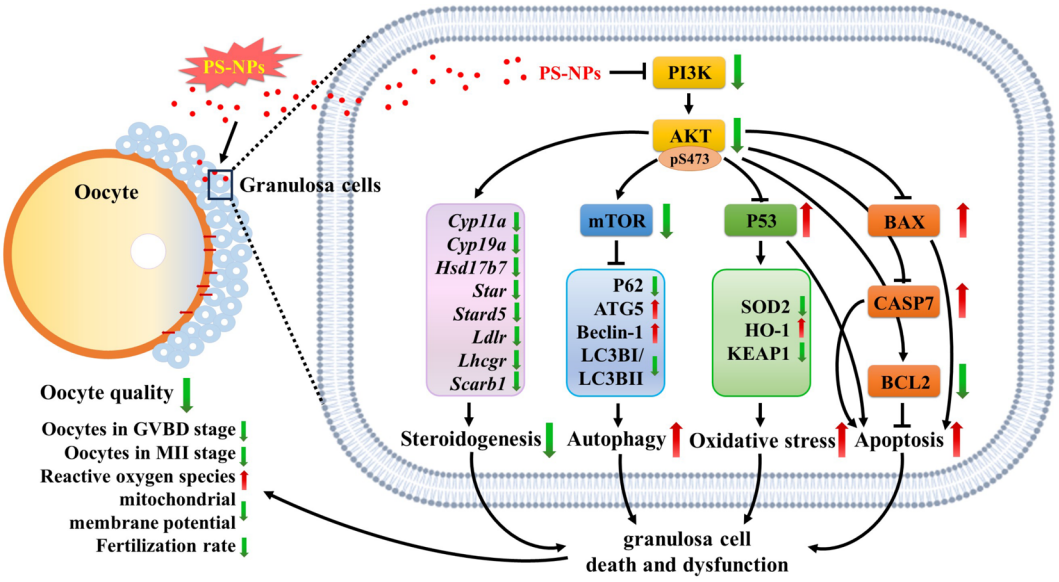

Fig. 10 Model of PI3K-AKT signaling pathway mediated dysfunction of granulosa cells induced by PS-NPs

and nucleus of the theca cells and granulosa cells, leading to ovarian cell apoptosis [58].Thus, the reduction in E2 levels in mouse serum following in vivo exposure to PS-NPs may be due to the combined dysfunction of both the theca cells and granulosa cells. However, in vitro experiments have shown that PS-NPs can still impair granulosa cell function and therefore impair E2 secretion even in the presence of testosterone. Collectively, these observations suggest that PS-NPs interfere with processes such as apoptosis, autophagy, and steroidogenesis in granulosa cells through the inhibition of the PI3K-AKT pathway, compromising the survival and functionality of these cells. Through a coculture system of granulosa cells and oocytes, we further verified that PS-NPs induced dysfunction of granulosa cells ultimately results in decreased oocyte quality and female fertility.

It is noteworthy that no abnormal development of primordial follicles was observed in our model mice. However, the initiation of follicle development is orchestrated by mTORC1 signaling in the pregranulosa cells [59]. Moreover, as a pivotal signaling pathway that governs oocyte activation, the up-regulation of PI3K activity stimulates the growth of dormant oocyte [60]. Due to our experiment involving prolonged exposure of sexually mature KM mice to PS-NPs, despite our findings of PI3K signaling pathway suppression in the mouse ovaries through sequencing, as the primary focus during this time is on the growth and development of follicles, only a few primordial follicles are gradually activated. Therefore, it is possible that the inhibition of the PI3K signaling pathway has a greater impact on the functionality of granulosa cells in growing follicles compared to the reduced activation of primordial follicles. Further validation is also needed in future work to use E2 antioxidant properties and PI3K-AKT activator to restore PS-NP-induced disruption of ovarian steroid production, oxidative stress, apoptosis, and autophagy in vivo mouse models [61].

Conclusions

This work demonstrates that PS-NPs induce apoptosis and autophagy in granulosa cells, and interfere with steroid hormone production, thereby impairing oocyte quality and reducing female fertility by inhibition of the PI3K-AKT signaling pathway in mice. Such discoveries illuminate the molecular mechanisms underlying the detrimental effects of PS-NPs on female reproductive health and emphasize potential intervention strategies to alleviate their adverse impact on female reproductive function.

Abbreviations

MNPs	Micro/nanoplastic
PS	Polystyrene
PI3K	Phosphatidylinositol-3-hydroxykinase
SP	Signaling pathway
RNA	Ribonucleic acid
FSH	Follicle stimulating hormone
LH	Luteinizing hormone
E2	17β-estradiol
O.C.T	Optimal Cutting Temperature
IU	International Units
PMSG	Pregnant mare serum gonadotropin
hCG	Human chorionic gonadotropin
GVBD	Germinal vesicle breakdown
MII	Metaphase II
ROS	Reactive oxygen species
MMP	Mitochondrial membrane potential
DEGs	Differentially expressed genes
KEGG	Kyoto Encyclopedia of Genes and Genomes
qPCR	Quantitative PCR
PI	Propidium iodide

CCK-8	Cell Counting Kit-8
IHC	Immunohistochemistry
PBS	Phosphate-buffered saline
IF	Immunofluorescence
DAPI	4′,6-diamidino-2-phenylindole
HTF	Human tubal fluid

Supplementary Information

The online version contains supplementary material available at https://doi.org/10.1186/s12951-024-02735-7.

Supplementary Material 1

Supplementary Material 2

Acknowledgements
The authors would like to thank Dr. Yuan-qiao He for help with mouse breeding and Dr. Wen Chen for providing technical guidance on the characterization of the PS-NPs. The authors also thank the online research drawing platform brgfx/Freepik (http://www.freepik.com) for scientific research drawings.

Author contributions
Yue Xue: Investigation, Formal analysis, Methodology, Data curation, Writing - original draft, Funding acquisition. Xiu Cheng: Investigation, Formal analysis, Methodology, Writing - original draft. Zhang-qiang Ma: Investigation, Formal analysis. Hou-peng Wang: Investigation, Formal analysis. Chong Zhou: Investigation. Jia Li: Investigation. Da-lei Zhang: Writing - review & editing. Liao-liao Hu: Investigation. Yan-fan Cui: Investigation. Jian Huang: Investigation. Tao Luo: Conceptualization, Supervision, Validation, Methodology, Writing - review & editing, Project administration, Funding acquisition. Li-ping Zheng: Conceptualization, Supervision, Validation, Methodology, Writing - review & editing, Project administration, Funding acquisition. The manuscript was written through contributions of all the authors. All the authors have approved the final version of the manuscript.

Funding
This work was supported by the Jiangxi Province Key Projects of Science and Technology Program of Traditional Chinese Medicine (2021Z019) to L.P.Z., the Natural Science Foundation of Jiangxi Province (20232ACB206008) to T.L., the Postgraduate Innovation Foundation of Nanchang University (YC2023-B040) to Y.X., the National Natural Science Foundation of China (82160284) to L.P.Z., and the Natural Science Foundation of Chongqing (GSTB2022NSCQ-MSX1381) to L.P.Z.

Data availability
No datasets were generated or analysed during the current study.

Declarations

Ethics approval and consent to participate
Not applicable.

Consent for publication
Not applicable.

Competing interests
The authors declare no competing interests.

Author details
[1]School of Basic Medical Sciences and School of Public and Jiangxi Provincial Key Laboratory of Preventive Medicine, Jiangxi Medical College, Nanchang University, Nanchang 330006, China
[2]School of Basic Medical Sciences, Jiangxi Medical College, Nanchang University; Institute of Biomedical Innovation, Jiangxi Medical College, Nanchang University, Nanchang 330031, China
[3]Jiangxi Provincial Key Laboratory of Disease Prevention and Public Health, Nanchang University, Nanchang 330006, China
[4]The 2nd affiliated hospital, Jiangxi Medical College, Nanchang University, Nanchang 330006, China

Received: 11 May 2024 / Accepted: 22 July 2024
Published online: 01 August 2024

References

1. Stubbins A, Law KL, Muñoz SE, Bianchi TS, Zhu L. Plastics in the Earth system. Volume 373. New York, NY: Science; 2021. pp. 655051–5.
2. Zhang K, Hamidian AH, Tubić A, Zhang Y, Fang JKH, Wu C, et al. Understanding plastic degradation and microplastic formation in the environment: a review. Environ Pollution (Barking Essex: 1987). 2021;274:116554.
3. Thompson RC, Olsen Y, Mitchell RP, Davis A, Rowland SJ, John AWG, et al. Lost at sea: where is all the plastic? Sci (New York NY). 2004;304(5672):838.
4. Atugoda T, Piyumali H, Wijesekara H, Sonne C, Lam SS, Mahatantila K, et al. Nanoplastic occurrence, transformation and toxicity: a review. Environ Chem Lett. 2023;21(1):363–81.
5. Yuan Y, Qin Y, Wang M, Xu W, Chen Y, Zheng L, et al. Microplastics from agricultural plastic mulch films: a mini-review of their impacts on the animal reproductive system. Ecotoxicol Environ Saf. 2022;244:114030.
6. Zhao X, Gao S, Ouyang D, Chen S, Qiu C, Qiu H, et al. Advances on micro/nanoplastics and their effects on the living organisms: a review. Sci Total Environ. 2023;904:166722.
7. da Costa JP, Santos PSM, Duarte AC, Rocha-Santos T. (Nano)plastics in the environment – sources, fates and effects. Sci Total Environ. 2016;566–567:15–26.
8. Priya AK, Jalil AA, Dutta K, Rajendran S, Vasseghian Y, Qin J, et al. Microplastics in the environment: recent developments in characteristic, occurrence, identification and ecological risk. Chemosphere. 2022;298:134161.
9. Prata JC, da Costa JP, Lopes I, Duarte AC, Rocha-Santos T. Environmental exposure to microplastics: an overview on possible human health effects. Sci Total Environ. 2020;702:134455.
10. Jin M, Wang X, Ren T, Wang J, Shan J. Microplastics contamination in food and beverages: direct exposure to humans. J Food Sci. 2021;86 7:2816–37.
11. Ibrahim YS, Tuan Anuar S, Azmi AA, Wan Mohd Khalik WMA, Lehata S, Hamzah SR, et al. Detection of microplastics in human colectomy specimens. JGH open: Open Access J Gastroenterol Hepatol. 2021;5(1):116–21.
12. Amato-Lourenço LF, Carvalho-Oliveira R, Júnior GR, Dos Santos Galvão L, Ando RA, Mauad T. Presence of airborne microplastics in human lung tissue. J Hazard Mater. 2021;416:126124.
13. Jenner LC, Rotchell JM, Bennett RT, Cowen M, Tentzeris V, Sadofsky LR. Detection of microplastics in human lung tissue using μFTIR spectroscopy. Sci Total Environ. 2022;831:154907.
14. Ragusa A, Svelato A, Santacroce C, Catalano P, Notarstefano V, Carnevali O, et al. Plasticenta: first evidence of microplastics in human placenta. Environ Int. 2021;146:106274.
15. Zhao Q, Zhu L, Weng J, Jin Z, Cao Y, Jiang H, et al. Detection and characterization of microplastics in the human testis and semen. Sci Total Environ. 2023;877:162713.
16. Hong Y, Wu S, Wei G. Adverse effects of microplastics and nanoplastics on the reproductive system: a comprehensive review of fertility and potential harmful interactions. Sci Total Environ. 2023;903:166258.
17. Huang T, Zhang W, Lin T, Liu S, Sun Z, Liu F, et al. Maternal exposure to polystyrene nanoplastics during gestation and lactation induces hepatic and testicular toxicity in male mouse offspring. Food Chem Toxicology: Int J Published Br Industrial Biol Res Association. 2022;160:112803.
18. Sun Z, Wen Y, Zhang F, Fu Z, Yuan Y, Kuang H, et al. Exposure to nanoplastics induces mitochondrial impairment and cytomembrane destruction in Leydig cells. Ecotoxicol Environ Saf. 2023;255:114796.
19. Liu Z, Zhuan Q, Zhang L, Meng L, Fu X, Hou Y. Polystyrene microplastics induced female reproductive toxicity in mice. J Hazard Mater. 2022;424 Pt C:127629.
20. Wei Z, Wang Y, Wang S, Xie J, Han Q, Chen M. Comparing the effects of polystyrene microplastics exposure on reproduction and fertility in male and female mice. Toxicology. 2022;465:153059.
21. Zeng L, Zhou C, Xu W, Huang Y, Wang W, Ma Z, et al. The ovarian-related effects of polystyrene nanoplastics on human ovarian granulosa cells and female mice. Ecotoxicol Environ Saf. 2023;257:114941.

22. An R, Wang X, Yang L, Zhang J, Wang N, Xu F, et al. Polystyrene microplastics cause granulosa cells apoptosis and fibrosis in ovary through oxidative stress in rats. Toxicology. 2021;449:152665.
23. Haddadi A, Kessabi K, Boughammoura S, Rhouma MB, Mlouka R, Banni M, et al. Exposure to microplastics leads to a defective ovarian function and change in cytoskeleton protein expression in rat. Environ Sci Pollut Res. 2022;29 23:34594–606.
24. Hou J, Lei Z, Cui L, Hou Y, Yang L, An R, et al. Polystyrene microplastics lead to pyroptosis and apoptosis of ovarian granulosa cells via NLRP3/Caspase-1 signaling pathway in rats. Ecotoxicol Environ Saf. 2021;212:112012.
25. Geng Y, Liu Z, Hu R, Huang Y, Li F, Ma W et al. Toxicity of microplastics and nanoplastics: invisible killers of female fertility and offspring health. Front Physiol. 2023;14.
26. Huang J, Zou L, Bao M, Feng Q, Xia W, Zhu C. Toxicity of polystyrene nanoparticles for mouse ovary and cultured human granulosa cells. Ecotoxicol Environ Saf. 2023;249:114371.
27. Yamochi T, Hashimoto S, Morimoto Y. Mural granulosa cells support to maintain the viability of growing porcine oocytes and its developmental competence after insemination. J Assist Reprod Genet. 2021;38 10:2591–9.
28. Matsuda F, Inoue N, Manabe N, Ohkura S. Follicular growth and atresia in mammalian ovaries: regulation by survival and death of granulosa cells. J Reprod Dev. 2012;58(1):44–50.
29. Senathirajah K, Attwood S, Bhagwat G, Carbery M, Wilson S, Palanisami T. Estimation of the mass of microplastics ingested - A pivotal first step towards human health risk assessment. J Hazard Mater. 2021;404(Pt B):124004.
30. Zuccarello P, Ferrante M, Cristaldi A, Copat C, Grasso A, Sangregorio D, et al. Exposure to microplastics (< 10 μm) associated to plastic bottles mineral water consumption: the first quantitative study. Water Res. 2019;157:365–71.
31. Nair AB, Jacob S. A simple practice guide for dose conversion between animals and human. J Basic Clin Pharm. 2016;7 2:27–31.
32. Xu W, Yuan Y, Tian Y, Cheng C, Chen Y, Zeng L, et al. Oral exposure to polystyrene nanoplastics reduced male fertility and even caused male infertility by inducing testicular and sperm toxicities in mice. J Hazard Mater. 2023;454:131470.
33. Sun D, Wang Y, Sun N, Jiang Z, Li Z, Wang L, et al. LncRNA DANCR counteracts premature ovarian insufficiency by regulating the senescence process of granulosa cells through stabilizing the interaction between p53 and hNRNPC. J Ovarian Res. 2023;16(1):41.
34. He H, Wang J, Mou X, Liu X, Li Q, Zhong M, et al. Selective autophagic degradation of ACLY (ATP citrate lyase) maintains citrate homeostasis and promotes oocyte maturation. Autophagy. 2023;19(1):163–79.
35. Xie HL, Wang YB, Jiao GZ, Kong DL, Li Q, Li H, et al. Effects of glucose metabolism during in vitro maturation on cytoplasmic maturation of mouse oocytes. Sci Rep. 2016;6:20764.
36. Kim D, Paggi JM, Park C, Bennett C, Salzberg SL. Graph-based genome alignment and genotyping with HISAT2 and HISAT-genotype. Nat Biotechnol. 2019;37:8.
37. Kim T, Seo HD, Hennighausen L, Lee D, Kang K. Octopus-toolkit: a workflow to automate mining of public epigenomic and transcriptomic next-generation sequencing data. Nucleic Acids Res. 2018;46 9:e53.
38. Pertea M, Pertea GM, Antonescu CM, Chang TC, Mendell JT, Salzberg SL. StringTie enables improved reconstruction of a transcriptome from RNA-seq reads. Nat Biotechnol. 2015;33(3):290–5.
39. Subramanian A, Tamayo P, Mootha VK, Mukherjee S, Ebert BL, Gillette MA, et al. Gene set enrichment analysis: a knowledge-based approach for interpreting genome-wide expression profiles. Proc Natl Acad Sci USA. 2005;102 43:15545–50.
40. Mao X, Cai T, Olyarchuk JG, Wei L. Automated genome annotation and pathway identification using the KEGG Orthology (KO) as a controlled vocabulary. Bioinf (Oxford England). 2005;21 19:3787–93.
41. Le M, Li J, Zhang D, Yuan Y, Zhou C, He J, et al. The emerging role of lysine succinylation in ovarian aging. Reproductive Biology Endocrinol. 2023;21 1:38.
42. Kato Y, Saga Y. Antagonism between DDX6 and PI3K-AKT signaling is an oocyte-intrinsic mechanism controlling primordial follicle growth†. Biol Reprod. 2023;109(1):73–82.
43. Li C, Qi T, Ma L, Lan YB, Luo J, Chu K, et al. In utero bisphenol A exposure disturbs germ cell cyst breakdown through the PI3k/Akt signaling pathway and BDNF expression. Ecotoxicol Environ Saf. 2023;259:115031.
44. Makker A, Goel MM, Mahdi AA. PI3K/PTEN/Akt and TSC/mTOR signaling pathways, ovarian dysfunction, and infertility: an update. J Mol Endocrinol. 2014;53(3):R103–18.
45. Kalous J, Aleshkina D, Anger M. A role of PI3K/Akt signaling in oocyte maturation and early embryo development. Cells. 2023;12:14.
46. Riley JK, Carayannopoulos MO, Wyman AH, Chi M, Ratajczak CK, Moley KH. The PI3K/Akt pathway is present and functional in the preimplantation mouse embryo. Dev Biol. 2005;284(2):377–86.
47. Wang H, Liang W, Wang X, Zhan Y, Wang W, Yang L, et al. Notch mediates the glycolytic switch via PI3K/Akt signaling to support embryonic development. Cell Mol Biol Lett. 2023;28(1):50.
48. Xiong X, Yang M, Hai Z, Fei X, Zhu Y, Pan B, et al. Maternal Kdm2a-mediated PI3K/Akt signaling and E-cadherin stimulate the morula-to-blastocyst transition revealing crucial roles in early embryonic development. Theriogenology. 2023;209:60–75.
49. Xie F, Zhang J, Zhai M, Liu Y, Hu H, Yu Z, et al. Melatonin ameliorates ovarian dysfunction by regulating autophagy in PCOS via the PI3K-Akt pathway. Reprod (Cambridge England). 2021;162(1):73–82.
50. Gong Y, Luo S, Fan P, Zhu H, Li Y, Huang W. Growth hormone activates PI3K/Akt signaling and inhibits ROS accumulation and apoptosis in granulosa cells of patients with polycystic ovary syndrome. Volume 18. Reproductive biology and endocrinology: RB&E; 2020. p. 1.
51. Chen YJ, Hsiao PW, Lee MT, Mason JI, Ke FC, Hwang JJ. Interplay of PI3K and cAMP/PKA signaling, and rapamycin-hypersensitivity in TGFbeta1 enhancement of FSH-stimulated steroidogenesis in rat ovarian granulosa cells. J Endocrinol. 2007;192:2405–19.
52. Hu Y, Xu J, Shi SJ, Zhou X, Wang L, Huang L, et al. Fibroblast growth factor 21 (FGF21) promotes porcine granulosa cell estradiol production and proliferation via PI3K/AKT/mTOR signaling. Theriogenology. 2022;194:1–12.
53. Jiang JY, Cheung CK, Wang Y, Tsang BK. Regulation of cell death and cell survival gene expression during ovarian follicular development and atresia. Front Bioscience: J Virtual Libr. 2003;8:d222–37.
54. Shao T, Ke H, Liu R, Xu L, Han S, Zhang X, et al. Autophagy regulates differentiation of ovarian granulosa cells through degradation of WT1. Autophagy. 2022;18 8:1864–78.
55. Lin M, Hua R, Ma J, Zhou Y, Li P, Xu X, et al. Bisphenol A promotes autophagy in ovarian granulosa cells by inducing AMPK/mTOR/ULK1 signalling pathway. Environ Int. 2021;147:106298.
56. Wei H, Qu L, Dai S, Li Y, Wang H, Feng Y, et al. Structural insight into the molecular mechanism of p53-mediated mitochondrial apoptosis. Nat Commun. 2021;12 1:2280.
57. Drane P, Bravard A, Bouvard V, May E. Reciprocal down-regulation of p53 and SOD2 gene expression-implication in p53 mediated apoptosis. Oncogene. 2001;20 4:430–9.
58. Hou CC, Zhu JQ. Nanoparticles and female reproductive system: how do nanoparticles affect oogenesis and embryonic development. Oncotarget. 2017;8 65:109799–817.
59. Adhikari D, Zheng W, Shen Y, Gorre N, Hämäläinen T, Cooney AJ, et al. Tsc/mTORC1 signaling in oocytes governs the quiescence and activation of primordial follicles. Hum Mol Genet. 2010;19 3:397–410.
60. Reddy P, Liu L, Adhikari D, Jagarlamudi K, Rajareddy S, Shen Y, et al. Oocyte-specific deletion of Pten causes premature activation of the primordial follicle pool. Volume 319 5863. New York, NY): Science; 2008. pp. 611–3.
61. Sobočanec S, Šarić A, Mačak Šafranko Ž, Popović Hadžija M, Abramić M, Balog T. The role of 17β-estradiol in the regulation of antioxidant enzymes via the Nrf2-Keap1 pathway in the livers of CBA/H mice. Life Sci. 2015;130:57–65.

Publisher's Note